INTERNATIONAL JOURNAL FOR NUMERICAL METHODS IN FLUIDS, VOL. 19, 905–938 (1994)

DYNAMIC VORTICITY CONDITION: THEORETICAL ANALYSIS AND NUMERICAL IMPLEMENTATION

JIE-ZHI WU, XIAO-HUI WU, HUI-YANG MA* AND JAIN-MING WU

The University of Tennessee Space Institute, Tullahoma, TN 37388, U.S.A.

SUMMARY

The dynamic boundary conditions for vorticity, derived from the incompressible Navier–Stokes equations, are examined from both theoretical and computational points of view. It is found that these conditions can be either local (Neumann type) or global (Dirichlet type), both containing coupling with the boundary pressure, which is the main difficulty in applying vorticity-based methods. An integral formulation is presented to analyse the structure of vorticity and pressure solutions, especially the strength of the coupling. We find that for high-Reynolds-number flows the coupling is weak and, if necessary, can be effectively bypassed by simple iteration. In fact, even a fully decoupled approximation is well applicable for most Reynolds numbers of practical interest. The fractional step method turns out to be especially appropriate for implementing the decoupled approximation. Both integral and finite difference methods are tested for some simple cases with known exact solutions. In the integral approach smoothed heat kernels are used to increase the accuracy of numerical quadrature. For the more complicated problem of impulsively started flow over a circular cylinder at $Re = 9500$ the finite difference method is used. The results are compared against numerical solutions and fine experiments with good agreement. These numerical experiments confirm our thoeretical analysis and show the advantages of the dynamic condition in computing high-Reynolds-number flows.

KEY WORDS Dynamic vorticity condition Theoretical analysis

1. INTRODUCTION

The boundary condition for vorticity at a solid surface is encountered in various vorticity-based formulations and numerical methods and is considered to be one of the most difficult problems in this area. In the past two decades great efforts have been made towards solving the problem; for recent reviews see References 1 and 2. In this paper we present a systematic examination of the problem from the viewpoint of dynamics rather than kinematics and thereby propose new algorithms. Here we briefly examine the root of the problem and introduce the main idea of this work.

Vorticity-based methods solve the vorticity equation under the *velocity* adherence condition on a solid surface. For incompressible flow, such a formulation avoids solving for the pressure while keeping the velocity solution divergence-free. However, in implementing these methods, one has to infer a boundary condition for vorticity from the velocity adherence, either by applying the Biot–Savart law to the solid surface or through a projection theorem.[1] This implies that in

* Permanent address: Department of Physics, The Graduate School of Academia Cinica, PO Box 3908, Beijing 100039, China.

CCC 0271–2091/94/220905–34

Received 5 November 1993
Revised 15 April 1994

its strict nature the vorticity boundary condition is of global type. Namely, the velocity no-slip imposes a *kinematic integral constraint* on the possible vorticity distribution in the flow domain rather than a local condition for the boundary behaviour of vorticity. Such an integral constraint cannot be easily included in a local algorithm (finite difference or finite element methods). Alternatively, this constraint can be represented as the differential relation between the velocity and vorticity, either by the Poisson equation or by a Cauchy–Riemann type of equation (see Reference 3 for some relevant theoretical clarification). Then the vorticity and velocity must be solved together, which results in a large coupled system of equations.

On the other hand, in the well-known fractional step approaches such as the integral formulation of J.-C. Wu and co-workers, where the kinematics and dynamics are treated sequentially in one time step;[4] or the vortex methods of Chorin and colleagues, where vorticity convection, creation and diffusion are implemented sequentially,[5] the vorticity field near the wall is simplified as a vortex sheet and hence the above volume integral constraint is reduced to a boundary integral equation or even a local condition for the vortex sheet strength (for the latter see also Section 2.3).

After the first draft of this paper was finished, the present authors became aware of the work of Koumoutsakos, Leonard and Pépin[6] (abbreviated as KLP below), which analysed the boundary conditions for viscous vortex methods. KLP noted that the above-mentioned vortex sheet strength can be manipulated so that a Dirichlet or Neumann type of condition can be modelled. They further pointed out that the Neumann type is better suited for vortex methods using the particle strength exchange (PSE) scheme. From a different approach we shall see that both types of condition can exist only in an *approximate sense*, though the (approximate) Neumann type of condition is better. The error of these approximations, however, has never been closely analysed.

Theoretically, the above difficulty reflects the basic fact that neither the local boundary vorticity nor its normal gradient can be rigorously inferred from any kinematic constraint derived from the velocity no-slip condition. Thus in the vorticity-based methods *it is impossible to obtain a strict Dirichlet or Neumann condition for the vorticity equation.* In this sense (within kinematics) we agree with Gresho's assertion[1] that 'there are no BCs on the vorticity'.

Moreover, the vorticity equation is one order higher than the Navier–Stokes equation, so an additional *compatibility condition* is necessary to exclude possible spurious solutions due to raising the equation's order, but again this condition is not derivable within kinematics.

The above observations motivated us to study a different approach. It can be outlined as follows.

The Navier–Stokes equation, with primitive variables $(\mathbf{u}, p)$ as unknowns, naturally matches the velocity adherence condition (but special consideration is necessary for the pressure boundary condition). By contrast, the vorticity equation, as the one-order-higher equivalent of the Navier–Stokes equation, does not. Rather, a natural boundary condition for vorticity should be a condition on velocity derivatives instead of velocity, and these derivatives are nothing but the fluid particles' acceleration on the solid wall. Then, as a constraint on the inertial force (per unit mass), the acceleration adherence implies a special force balance on the wall through the Navier–Stokes equation, which in turn gives the exact expressions for the normal gradient of vorticity ω and pressure p and have the Newmann conditions for second-order vorticity and pressure equations. These *dynamic conditions* are the subject of the present paper.

While such a 'derivative argument' is well known in other contexts, Anderson[7] was the first to apply it to the vorticity boundary condition problem. He derived an integral–differential equation which determines the boundary value of vorticity. See also the paper of Anderson and Reider[8] (abbreviated as AR below) for a recent application of this condition. Here, from a different point of view, we present a systematic theoretical analysis for both the dynamic vorticity boundary conditions and the compatibility conditions. Numerical schemes are then designed

based on the theoretical understanding, and checked against exact analytical solutions, highly accurate numerical solutions and fine experiments.

The contents of this paper are arranged as follows. In Section 2 we state the general dynamic boundary conditions for ω and p and prove that they contain the compatibility conditions as well. The detailed structure of solutions of ω and p is studied via corresponding dynamic integral formulations, which also provides a common theoretical basis for various integral methods. The dynamic theory reveals the inherent (ω, p) coupling due to the no-slip condition at the solid wall and that such coupling makes it generally impossible to prescribe local vorticity boundary conditions without knowing the tangential gradient of the boundary pressure. However, with the help of the dynamic integral formulation we are able to study the 'strength' of the (ω, p) coupling, which serves as the basis for the design of new finite difference techniques in later sections. In particular, we prove that in fractional step methods the strength of the (ω, p) coupling is reduced to an order of the $-\frac{1}{2}$ power of the Reynolds number. Section 3 presents numerical tests against some known exact solutions where the (ω, p) coupling is absent. Smoothed heat kernels are introduced for integral methods and a finite difference scheme is also tested with different treatments of the boundary conditions. Section 4 presents our numerical results for the impulsively started flow over a circular cylinder at $Re = 9500$. A finite difference scheme based on the fractional step approach is used. The results reveal that the (ω, p) coupling is already so weak that, within the second-order discretization error, the fully decoupled approximation can predict a flow field almost identical with that obtained with recovered coupling by iteration. Some concluding remarks are made in Section 5.

2. THEORETICAL ANALYSIS

Consider an incompressible flow of unit density past a solid body. Let the flow domain be V with boundary ∂V moving with velocity $\mathbf{b}$. For neatness denote

$$\mathscr{L}(\mathbf{u}) = \mathbf{a} - \nu\nabla^2\mathbf{u} = \frac{\partial \mathbf{u}}{\partial t} + \mathbf{u}\cdot\nabla\mathbf{u} - \nu\nabla^2\mathbf{u}, \tag{1}$$

where $\mathbf{a} = \mathrm{D}\mathbf{u}/\mathrm{D}t$ is the acceleration, such that the Navier–Stokes and continuity equations read

$$\mathscr{L}(\mathbf{u}) + \nabla p = 0 \quad \text{and} \quad \nabla\cdot\mathbf{u} = 0. \tag{2a,b}$$

The initial and boundary conditions are

$$\mathbf{u} = \mathbf{u}_0 \quad \text{at } t = 0 \quad \text{in } V, \tag{2c}$$

$$\mathbf{n}\times\mathbf{u} = \mathbf{n}\times\mathbf{b} \quad \text{and} \quad \mathbf{n}\cdot\mathbf{u} = \mathbf{n}\cdot\mathbf{b} \quad \text{on} \quad \partial V. \tag{2d,e}$$

Hereafter $\mathbf{n}$ is the unit normal vector on the boundary ∂V pointing out of the fluid. The boundary ∂V may consist of a solid surface B and an infinite boundary ∂V_∞. In the latter case we can still imagine an 'adherence' there, since (2d,e) apply as well, with $\mathbf{b}$ being assumed as a uniform vector, say $\mathbf{U}(t)$. Then, instead of solving problem (2) in terms of primary variables, the vorticity-based methods seek the solution of

$$\nabla\times\mathscr{L}(\mathbf{u}) = \mathscr{N}(\mathbf{u}, \boldsymbol{\omega}) = 0, \qquad \boldsymbol{\omega} = \nabla\times\mathbf{u}, \tag{3a,b}$$

under constraints (2b–e). As long as this problem is well posed and its solution $\mathbf{u}$ obtained, then there must be

$$\mathscr{L}(\mathbf{u}) + \nabla\phi = 0$$

for some ϕ, which can only be identified as the pressure p. Therefore, if problem (3) and (2b–e) can be solved satisfactorily, there is no need to solve for p simultaneously. However, although conditions (2b) and (3b) can be easily ensured by using the streamfunction or Biot–Savart law, and (2e) can be satisfied by superposing a potential flow, difficulty arises in implementing (2d) directly in terms of $\boldsymbol{\omega}$. This motivated us to turn to the dynamic boundary conditions. In this section we develop the relevant general theory.

2.1. *Dynamic Neumann conditions for the* $(\boldsymbol{\omega}, p)$ *field*

It is easy to understand that the velocity adherence implies *acceleration adherence*, i.e.

$$\mathbf{n} \times \mathbf{a}_B = \mathbf{n} \times \mathbf{a}_b \quad \text{and} \quad \mathbf{n} \cdot \mathbf{a}_B = \mathbf{n} \cdot \mathbf{a}_b, \quad t \geq 0, \tag{4a,b}$$

where $\mathbf{a}_b$ is the wall acceleration and (also below) the subscript B implies the value of fluid quantities on the solid surface B. To recover (2d,e), one simply adds an initial velocity adherence[7,9]

$$\mathbf{n} \times \mathbf{u}_B = \mathbf{n} \times \mathbf{b} \quad \text{and} \quad \mathbf{n} \cdot u_B = \mathbf{n} \cdot \mathbf{b}, \quad t = 0. \tag{5a,b}$$

Note that, as shown by Wu and Wu,[10] in *vorticity-based formulations* the no-slip condition should be and can be imposed at $t = 0$, even if there is an (idealized) impulsive start from a potential flow along with a singular vortex sheet on B, since only the no-slip condition can determine the sheet strength (see also Section 2.2 below). However, in the $(\mathbf{u}, p)$ formulation there is no such need and it is all right to impose no slip only for $t > 0$ as Gresho[1,2] stressed.

Now the local dynamic boundary conditions of the Neumann type for $\boldsymbol{\omega}$ and p follow from applying (2a) to the wall and using (5a,b). It is then immediately clear that once these dynamic boundary conditions are used in solving the vorticity field, the $(\boldsymbol{\omega}, p)$ coupling becomes inevitable. Thus, theoretically, one has to solve the $(\boldsymbol{\omega}, p)$ equations simultaneously. Symbolically, these equations and repsective dynamic boundary conditions are

$$\nabla \times \mathscr{L}(\mathbf{u}) = 0, \qquad \mathbf{n} \times \mathscr{L}(\mathbf{u})_B = -\mathbf{n} \times \nabla p_B, \tag{6a,b}$$

$$\nabla^2 p = -\nabla \cdot \mathscr{L}(\mathbf{u}), \qquad \left(\frac{\partial p}{\partial n}\right)_B = -\mathbf{n} \cdot \mathscr{L}(\mathbf{u})_B. \tag{7a,b}$$

We shall see below that like (7b), equation (6b) can be cast into an explicit formula for the *boundary vorticity flux* $\boldsymbol{\sigma} = \nu(\partial\boldsymbol{\omega}/\partial n)_B$. Equations (4a,b) are necessary in fixing $(\partial\boldsymbol{\omega}/\partial n)_B$ and $(\partial p/\partial n)_B$, respectively.

Our first concern is whether the solution to this set of equations is also a solution of the original equation (2). We have the following.

Theorem 1

Assume that $\mathbf{u}$ satisfies (6a) and (7a). Then it is the solution of (2a) if either (6b) or (7b) holds.

Proof. From (6a) we have $\mathscr{L}(\mathbf{u}) + \nabla\phi = 0$ for some ϕ. Substituting this into (7a), we get

$$\nabla \cdot \nabla(p - \phi) = \nabla^2 \phi' = 0 \tag{8}$$

for $\phi' = p - \phi$. However, (6b) implies $\mathbf{n} \times \nabla\phi' = 0$ or $\phi' = \text{const.}$ on B, so $\nabla\phi' = 0$ in V.

Alternatively, (7b) implies $\partial\phi'/\partial n = 0$ on B and the same result follows. In both cases (2a) holds. □

Therefore, by introducing acceleration adherence (4a,b), the boundary conditions and compatibility conditions are merged into one. In this case (6b) and (7b) represent the mathematically natural boundary conditons for ω and p respectively. They are also physically natural: as shown by Wu and Wu[10] (see also Section 2.2 below), they precisely reflect the physics of (ω, p) creation from the wall.

The above theorem can be restated as follows.

Corollary 1

Let $\mathbf{u}$ be a solution of problem (6a,b) (or (7a,b)). Then it is also a solution of (2a) if and only if it satisfies (7a) (or (6a)) simultaneously.

Proof. The 'only if' part is trivial. To prove the 'if' part, for example, from (6a, b) we obtain $\mathscr{L}(\mathbf{u}) = -\nabla\phi$ with $\mathbf{n} \times \nabla(\phi - p) = 0$, but by (7a) we must have $\nabla^2(\phi - p) = 0$. The rest of the proof is obvious. □

As mentioned before, once the velocity field of an incompressible flow has been solved by whatever method, ∇p can be inferred from the Navier–Stokes equation (2a), but this involves an inconvenient computation of $\partial\mathbf{u}/\partial t$. Solving the second-order pressure equation (7a,b) avoids this problem. However, Corollary 1 shows that this approach needs to satisfy the vorticity equation as a prerequisite. Similarly, solving the vorticity equation (6a, b) also requires the second-order pressure equation.

Problems (6a,b) and (7a,b), along with initial condition (2c) plus a given initial vorticity distribution $\boldsymbol{\omega}_0$ in V at $t = 0$, constitute a well-posed initial–boundary value problem for the coupled (ω, p) field. The pressure part of this problem has been extensively studied by Gresho and Sani,[11] so we shall mainly concentrate on the vorticity part of the problem. However, the (ω, p) coupling on B, and hence an interior (ω, p) coupling over the whole flow domain V, should not be ignored or oversimplified. The effect of this coupling will be analysed theoretically in Section 2.2 and numerical aspects of handling this coupling will be presented in Section 2.3.

We now recover the detailed form of equations and boundary conditions. For incompressible flow the (ω, p) equations (6a) and (7a) read

$$\frac{\partial\boldsymbol{\omega}}{\partial t} + \nabla \times \mathbf{L} - \nu\nabla^2\boldsymbol{\omega} = 0, \qquad \mathbf{L} \equiv \boldsymbol{\omega} \times \mathbf{u}, \tag{9}$$

$$\nabla^2 p_0 = -\nabla \cdot \mathbf{L}, \qquad p_0 \equiv p + \tfrac{1}{2}|\mathbf{u}|^2. \tag{10}$$

The general formula for the boundary vorticity flux $\boldsymbol{\sigma}$ on a solid wall, as well as that for the normal pressure gradient, has been given by Wu,[12] Wu *et al.*[13] and Wu and Wu.[10] The incompressible version reads

$$\boldsymbol{\sigma} \equiv \nu\left(\frac{\partial\boldsymbol{\omega}}{\partial n}\right)_B = \mathbf{n} \times \mathbf{a}_b + (\mathbf{n} \times \nabla) \cdot (p_B\mathbf{I} + \nu\boldsymbol{\omega}'_B \times \mathbf{nn}), \tag{11}$$

$$\delta \equiv -\left(\frac{\partial p}{\partial n}\right)_B = \mathbf{n} \cdot \mathbf{a}_b + (\mathbf{n} \times \nabla) \cdot \nu\boldsymbol{\omega}_B, \tag{12}$$

where $\mathbf{I}$ is the unit tensor and $\boldsymbol{\omega}'_B = \boldsymbol{\omega}_B - 2\boldsymbol{\Omega}(t)$ is the relative vorticity, with $\boldsymbol{\Omega}$ being the angular velocity of the wall. The two-dimensional form of these formulae is well known, while in three dimensions there is an extra term $(\mathbf{n} \times \nabla) \cdot (\nu\boldsymbol{\omega}'_B \times \mathbf{nn})$ in $\boldsymbol{\sigma}$, indicating its dependence on $\boldsymbol{\omega}_B$ or skin friction $\boldsymbol{\tau}_B = \nu\mathbf{n} \times \boldsymbol{\omega}'_B$ and the surface curvature.[10,12,13] The physical aspects of $\boldsymbol{\sigma}$ have been discussed by Wu and Wu[10] in depth, where it is also shown that this flux, first introduced by Lighthill,[14] is the unique correct measure of vorticity source strength on a solid wall.

2.2. *The solution structure of vorticity*

We now examine the detailed structure of formal $(\boldsymbol{\omega}, p)$ solutions by the standard Green function method. This study provides a foundation for the later design of numerical (both integral and local) schemes.

We first concentrate on the vorticity part and assume temporarily that the p_B distribution is known. Let $\mathbf{r} = \mathbf{x} - \boldsymbol{\xi}$, $r = |\mathbf{r}|$, and

$$G^*(\mathbf{x}, \boldsymbol{\xi}; t, \tau) = \frac{H(t-\tau)}{[4\pi\nu(t-\tau)]^{d/2}} \exp\left(-\frac{r^2}{4\nu(t-\tau)}\right) \tag{13}$$

be the fundamental solution of the heat equation in free space, with H being the step function and d the spatial dimensionality. From Green's second identity it follows that

$$\boldsymbol{\omega}(\mathbf{x}, t) = \int_V G_0^* \boldsymbol{\omega}_0 \, dV + \int_0^t d\tau \oint_B \left(G^* \boldsymbol{\sigma} - \nu\boldsymbol{\omega}_B \frac{\partial G^*}{\partial n}\right) dS - \int_0^t d\tau \oint_B G^* \mathbf{n} \times \mathbf{L}_B \, dS + \int_0^t d\tau \int_V \nabla G^* \times \mathbf{L} \, dV. \tag{14}$$

Here the subscript zero implies values at $\tau = 0$ and $\boldsymbol{\sigma}$ is as given by (11). The first volume integral represents the effect of initial $\boldsymbol{\omega}$ distribution and the last two represent the non-linear convection effect. The $\partial G^*/\partial n$ term can be eliminated if the Green function with zero normal derivative can be found. For simple boundaries such as a flat plate or a circular cylinder this can be achieved by using the image method.

Note that great care is necessary in determining the effect of a moving boundary. Although velocity adherence implies acceleration adherence, in the Eulerian description the local and convection accelerations of fluid particles on B, $(\partial\mathbf{u}/\partial t)_B$ and $(\mathbf{u} \cdot \nabla\mathbf{u})_B$, are not equal to those of the solid surface, $\partial\mathbf{b}/\partial t$ and $\mathbf{b} \cdot \nabla\mathbf{b} = \boldsymbol{\Omega} \times \mathbf{b}$ respectively. Rather, it can be shown that

$$\left(\frac{\partial\mathbf{u}}{\partial t}\right)_B = \frac{\partial\mathbf{b}}{\partial t} - (\mathbf{n} \cdot \mathbf{b})(\boldsymbol{\omega}'_B \times \mathbf{n}), \qquad (\mathbf{u} \cdot \nabla\mathbf{u})_B = \boldsymbol{\Omega} \times \mathbf{b} + (\mathbf{n} \cdot \mathbf{b})(\boldsymbol{\omega}'_B \times \mathbf{n}).$$

Moreover, a normal motion of B will generally lead to a time dependence of the normal vector $\mathbf{n}$ and the flow domain V. All these make flow problems with moving walls (e.g. an oscillating flap) much more complicated than those with stationary walls. For an analysis of the effect of a moving boundary on the time-averaged vorticity flux see Reference 15. For simplicity we assume $\mathbf{n} \cdot \mathbf{b} = 0$ in the rest of the paper. Thus

$$\mathbf{n} \times \mathbf{L}_B = -\mathbf{bn} \cdot \boldsymbol{\omega}_B = -2\mathbf{bn} \cdot \boldsymbol{\Omega}.$$

As shown by Wu and Wu,[10] if in an idealized model the flow is started by either an *impulsive*

pressure gradient and/or an *impulsive* body motion, the boundary vorticity flux σ must contain a δ-function at $t = 0$ and creates an infinitely thin vortex sheet with strength γ_0:

$$\sigma = \mathbf{n} \times (\mathbf{b}_0 - \mathbf{u}_0)\delta(t) = \gamma_0 \delta(t), \quad 0^- \leq t \leq 0^+, \tag{15}$$

where $\mathbf{u}_0$ denotes a suddenly gained flow velocity above the wall at $t = 0$ due to the impulsive pressure gradient. In (14) this singular behaviour of σ can be easily separated from its regular part:

$$\oint_0^t d\tau \oint_B G^* \sigma \, dS = \oint_B G_0^* \gamma_0 \, dS + \int_{0^+}^t d\tau \oint_B G^* \sigma \, dS. \tag{16}$$

Note that the initial velocity no-slip condition has been implied through (16); without such a condition the initial vortex sheet strength γ_0 would be uncertain and have to be prescribed in advance.

To illustrate the implication of (14), we apply it to a unidirectional flow $u(y, t)$ over a flat plate at $y = 0$. Assume that the fluid and wall are at rest for $t < 0$. Take $d = 1$ and $r = y - \eta$ in (13) and eliminate $\partial G^*/\partial n$ in (14) by the method of images. Then we readily obtain

$$\omega(y, t) = \frac{\gamma_0}{\sqrt{(\pi \nu t)}} \exp\left(-\frac{y^2}{4\nu t}\right) + \int_{0^+}^t \frac{\sigma(\tau)}{\sqrt{[\pi \nu (t - \tau)]}} \exp\left(-\frac{y^2}{4\nu(t - \tau)}\right) d\tau, \tag{17a}$$

where $\gamma_0 = b_0 - u_0$ and

$$\sigma(t) = \frac{db}{dt} + P(t), \tag{17b}$$

with $P(t) \equiv \partial p/\partial x$ that can only be a function of t. In particular, the boundary vorticity is

$$\omega_B(t) = \frac{\gamma_0}{\sqrt{(\pi \nu t)}} + \frac{1}{\sqrt{(\pi \nu)}} \int_{0^+}^t \frac{\sigma(t)}{\sqrt{(t - \tau)}} d\tau. \tag{18}$$

For example, the solution of the Stokes first problem (the Rayleigh problem) simply follows from letting $\sigma = 0$ for $t \geq 0^+$ in (17a) and (18), yielding the boundary vorticity

$$\omega_B = \frac{\gamma_0}{\sqrt{(\pi \nu t)}}. \tag{19}$$

Alternatively, if $P(t) = u_0 = 0$ but $b = b_0 \cos t$, say, (18) yields

$$\omega_B = \frac{b_0}{\sqrt{(\pi \nu t)}} + b_0 \sqrt{\left(\frac{2}{\nu}\right)} [S(\sqrt{t}) \cos t - C(\sqrt{t}) \sin t], \tag{20}$$

where $S(x)$ and $C(x)$ are Fresnel functions. This is the solution of the generalized Stokes second problem including the transient effect, which has been thoroughly studied by Panton.[16] As $t \to \infty$, equation (20) gives the classical result $\omega_B(t) = (b_0/\sqrt{\nu}) \cos(t + \pi/4)$. In Section 3 we shall give numerical results for these two typical problems as the first test of the numerical algorithms, but the flat plate is replaced by a circular cylinder.

The special case with $b = 0$ and $P = \text{const.}$ in (17) was used by Gresho[1] to explain the singular behaviour of ω_B and σ at $t = 0$. He concludes that the vortex sheet 'is a primary evil when using vorticity-based methods'. However, this evil disappears in the integral formulation.

Note that in the above example, there is no way to infer the boundary condition in advance from kinematic relations only (either theoretically or numerically), since the effect of p is 'unknown' in the kinematics. This statement is also valid for general *gradually* started flows owing to the sudden appearance of a *finite* pressure gradient. This is another indication that vorticity creation can only be fully understood dynamically.

We now return to (14) and further confine ourselves to the case with $\mathbf{b} = 0$ and hence $\mathbf{n} \cdot \boldsymbol{\omega}_B = 0$ for neatness. By (11) we have

$$G^*\boldsymbol{\sigma} = (\mathbf{n} \times \nabla) \cdot [G^*(p_B\mathbf{I} + \nu\boldsymbol{\omega}_B \times \mathbf{nn})] - (\mathbf{n} \times \nabla G^*) \cdot (p_B\mathbf{I} + \nu\boldsymbol{\omega}_B \times \mathbf{nn}).$$

Here, owing to a consequence of the generalized Stokes theorem

$$\oint (\mathbf{n} \times \nabla) \circ \mathscr{F}\, \mathrm{d}S = 0 \tag{21}$$

for any tensor $\mathscr{F}$ and meaningful operation $\circ$, the first term of $G^*\boldsymbol{\sigma}$ has no contribution to its surface integral, while the second term is

$$-(\mathbf{n} \times \nabla G^*) \cdot (p_B\mathbf{I} + \nu\boldsymbol{\omega}_B \times \mathbf{nn}) = \nabla G^* \times \mathbf{n}p + \mathbf{n}\nabla G^* \cdot \nu\boldsymbol{\omega}_B.$$

Therefore, since

$$\mathbf{n}p_B + \mathbf{n} \times \nu\boldsymbol{\omega}_B = \mathbf{t}_B \tag{22a}$$

is the wall stress, it follows from (14) and (16) that for stationary B

$$\boldsymbol{\omega}(\mathbf{x}, t) = \oint_B G_0^*\boldsymbol{\gamma}_0\, \mathrm{d}S + \int_V G_0^*\boldsymbol{\omega}_0\, \mathrm{d}V + \int_{0^+}^t \mathrm{d}\tau \oint_B \nabla G^* \times \mathbf{t}_B\, \mathrm{d}S + \int_0^t \mathrm{d}\tau \int_V \nabla G^* \times \mathbf{L}\, \mathrm{d}V. \tag{22b}$$

We make three remarks on (22). First, although in deriving (22b) we only used the free space Green functions (13), the $G^*\partial\boldsymbol{\omega}/\partial n$ term is remarkably absent in the surface integral. Thus, along with the corresponding pressure equation (25) below, we arrive at an innovative integral formulation of a *Dirichlet problem with free space Green function*. However, this problem is not for $\boldsymbol{\omega}$ alone; rather, it is for the coupled $(\boldsymbol{\omega}, p)$. Second, since by (13) ∇G^* is along the direction of $\mathbf{r} = \mathbf{x} - \boldsymbol{\xi}$, we see that the boundary stress $\mathbf{t}_B$ at a point $\boldsymbol{\xi}_B \in B$ affects the vorticity field at a point $\mathbf{x} \in V$ only by its components *perpendicular* to $\mathbf{r}$, through diffusion. Third, applying (22b) to B implies a dynamic integral constraint on the boundary vorticity $\boldsymbol{\omega}_B$, or a global and implicit Dirichlet condition for $\boldsymbol{\omega}$ in V. Unlike the boundary vorticity flux $\boldsymbol{\sigma}$, however, there exists no local equation for $\boldsymbol{\omega}_B$. This is factually a mathematical manifestation of the underlying physics:[10] it is the boundary vorticity flux rather than the boundary vorticity that reflects the vorticity source directly, and the boundary vorticity itself arises through a time-accumulated effect of the flux (see (18)).

We use the integral formulation here mainly for clarifying the structure of the solution and the effect of boundary conditions. In numerical computations integral methods are usually more time-consuming than finite difference methods. However, owing to the desire to remove the less accurate random walk approach from Chorin's vortex methods, some authors have recently turned to deterministic diffusion algorithms, which are mostly of integral type, since then a smooth connection between the Lagrangian convection substep and the Eulerian diffusion substep can be achieved (in contrast, to connect a Lagrangian convecton and a finite difference diffusion, one has to use the vortex-in-cell technique at the expense of artificial viscosity). For example, the PSE method (see References 6 (KLP), 17 and 18 and references cited therein) uses an approximate estimation of $\boldsymbol{\sigma}$ as the Neumann condition, and to avoid the appearance of $\boldsymbol{\omega}_B$,

it starts from Green's first identity instead of (14), bringing about some error due to the inevitable appearance of a volume integral of a Taylor expansion[19] (also A. Leonard, personal communication 1991). On the other hand, Lu and Ross[20] use an integral equation for ω_B to construct the Dirichlet condition, and introduce an approximate image Green function (with respect to a flat plate) to remove the vorticity flux σ. Now, despite the large consumption of computational resource inherent in these integral methods, we believe that (14) and (22) provide a foundation for deterministic diffusion methods.

2.3. *Boundary pressure and decoupled approximation*

So far we have assumed that p_B is known in (11) or (22). We now turn to the pressure problem (10), (12), which in turn depends on ω_B. This can also be seen clearly from the solution structure for p. Let

$$G(\mathbf{x}, \xi) = \begin{cases} -\ln r/2\pi & \text{if } d = 2 \\ 1/4\pi r & \text{if } d = 3 \end{cases} \tag{23}$$

be the fundamental solution of the Laplace equation in free space. Similarly to (14), from Green's second identity it readily follows that the stagnation pressure p_0 is given by

$$p_0(\mathbf{x}) = -\oint_B \left(G\delta + p_0 \frac{\partial G}{\partial n} \right) dS + \oint_B G\mathbf{n} \cdot \mathbf{L}_B \, dS - \int_V \nabla G \cdot \mathbf{L} \, dV, \tag{24}$$

where δ is as given by (12). Hence, substituting (12) into (24) and using (21), for a stationary wall we find that the counterpart of (22) is

$$p_0(\mathbf{x}) = -\oint_B \nabla G \cdot \mathbf{t}_B \, dS - \int_V \nabla G \cdot \mathbf{L} \, dV, \tag{25}$$

where $\mathbf{t}_B$ is as defined by (22a). It follows from (25) that the component of $\mathbf{t}_B$ *parallel* to $\mathbf{r} = \mathbf{x} - \xi$ at $\xi_B \in B$ has an effect on p_0 at $\mathbf{x}$. Again equation (25) contains a boundary integral equation for p_B ($p_0 = p$ on stationary B).

In principle, p_B or its tangential gradient can be solved simultaneously with the vorticity. However, such a global coupling is computationally undesirable, especially for vortex methods, since otherwise the methods would lose one of their main advantages, i.e. getting rid of p and working in the rotational flow region only. In many $(\omega, \mathbf{u})$-based methods ω is solved coupled with $\mathbf{u}$ through the no-slip condition. This certainly avoids solving p, but it only switches the coupling from dynamics to kinematics.

The fractional step (or operator-splitting) methods can partially but greatly reduce the (ω, p) coupling. In these methods one solves the Euler and Stokes equations

$$\frac{\partial \mathbf{u}_1}{\partial t} + \mathbf{u}_1 \cdot \nabla \mathbf{u}_1 + \nabla p_1 = 0, \tag{26a}$$

$$\frac{\partial \mathbf{u}_2}{\partial t} + \nabla p_2 = \nu \nabla^2 \mathbf{u}_2 \tag{26b}$$

successively for each time step. Here the scalars p_1 and p_2 are necessary to guarantee the solenoidal condition (2b). Symbolically, the solution of the Navier–Stokes equation (2a) can be written as

$$\mathbf{u}(\Delta t) = S(\Delta t)\mathbf{u}^0 = H(\Delta t)E(\Delta t)\mathbf{u}^0,$$

where $\mathbf{u}^0$ is the initial velocity for a time step and $S(t)$, $H(t)$ and $E(t)$ are the solution operators for the Navier–Stokes, Stokes and Euler equations respectively. Beale and Greengard[21] proved that this scheme is convergent and first-order-accurate in time (higher-order schemes can be designed, e.g. the Strang splitting scheme). It should be mentioned that while $\mathbf{u}_2$ (solved from (26b) with $\mathbf{u}_1$ as the initial condition) is a valid approximation of the original Navier–Stokes equation, it remains unclear whether the same is true for p_2. In fact, equation (26b) shows that p_2 satisfies the Laplace equation, whose solution may be qualitatively different from that of (10).

Corresponding to (26a, b), we have

$$\frac{\partial \boldsymbol{\omega}_1}{\partial t} + \nabla \times \mathbf{L}_1 = 0, \qquad \mathbf{L}_1 = \boldsymbol{\omega}_1 \times \mathbf{u}_1, \tag{27a}$$

$$\frac{\partial \boldsymbol{\omega}_2}{\partial t} = \nu \nabla^2 \boldsymbol{\omega}_2, \tag{27b}$$

as the vorticity convection and diffusion equations. Note that $\boldsymbol{\omega}_1$ and p_1 are fully *decoupled* in (27a), since only (2e) is required on B. In other words, equations (27a) can be solved without invoking p, and in this substep there is no need for the vorticity boundary condition (BC) at all. Here Lagrangian vortex methods exhibit most of their strength. On the other hand, the coupling between ω_2 and p_2 persists in (27b) owing to the no-slip condition, which causes the problem of vorticity BCs. Thus, as Gresho[22] observed, the Stokes part is most difficult to deal with. Now the coupling is revealed by the reduced version of (22) and (25), i.e.

$$\boldsymbol{\omega}_2(\mathbf{x}, t) = \oint_B G_0^* \boldsymbol{\gamma}_0 \, \mathrm{d}S + \int_V G_0^* \boldsymbol{\omega}_{20} \, \mathrm{d}V + \int_{0^+}^{t} \mathrm{d}\tau \oint_B \nabla G^* \times \mathbf{t}_{2B} \, \mathrm{d}S, \tag{28}$$

$$\tfrac{1}{2} p_{2B} + \oint_B \nabla G \cdot (\mathbf{n} p_{2B} + \mathbf{n} \times \nu \boldsymbol{\omega}_{2B}) \, \mathrm{d}S = 0. \tag{29}$$

Here the integral in (29) should be understood in the sense of the Cauchy principal value. Note that $\mathbf{t}_{2B}$ is defined by (22a), so (28) alone is not solvable because of unknown p_{2B}. Equations (28) and (29) have to be solved together.

Two benefits can be seen from (28) and (29). First, the equations are linearly coupled, which makes them easier to solve. Second, the velocity does not appear in the coupling, so it can be solved separately after $\boldsymbol{\omega}$ is obtained.

In the original Chorin-Marsden product formula[23] the solution operator is approximated by

$$S(\Delta t) = H(\Delta t) \Phi(\Delta t) E(\Delta t),$$

where $\Phi(t)$ is called the 'vorticity creation operator'. The effect of this operator is to *model* vorticity creation from a solid wall and hence provide approximate local vorticity BCs for $H(t)$. Usually the modelling does not use the information of pressure directly and so $\boldsymbol{\omega}$ is decoupled from p. This in fact is also true for the local kinematic vorticity BCs in conventional finite-difference methods.

The modelling of vorticity creation can only be approximate and has very often been based on intuition. After the substep of inviscid convection (i.e. solving (27a)) a slip velocity $\mathbf{u}_s$ always appears on the solid boundary B. Thus, like (16), there must be a singular vortex sheet with strength

$$\boldsymbol{\gamma} = \mathbf{n} \times (\mathbf{b} - \mathbf{u}_s).$$

This vortex sheet is then used either to estimate the variation in boundary vorticity (i.e. a Dirichlet condition),

$$\Delta\omega_B \approx \frac{\gamma}{h}, \tag{30}$$

with h being a chosen small normal distance,[4] or to determine the circulation of the discrete vortices newly created from B.[5] One common choice is to set $h = \sqrt{(\pi\nu\Delta t)}$, implying that (19) is used to approximate ω_B everywhere, and some dynamics is thereby introduced. We see that this choice is essentially a local unidirectional flow approximation.

Another way of utilizing γ is the dynamic approach that has been applied in some ω-based methods.[6,18,24] The following Neumann condition is adopted (the argument leading to this will be given later):

$$\sigma \approx \frac{\gamma}{\Delta t}. \tag{31}$$

Equations (30) and (31) are both decoupled from the pressure and hence are *not exact*. It should be stressed that the reverse reasoning that (30) and (31) imply no explicit coupling between ω and p is incorrect.

Both (30) and (31) are often criticized as being inaccurate. However, because of the singularity and the 'unusual' way of computing the BCs, the error estimate is not so straightforward. As we discussed above, the vorticity creation and diffusion are not really separable because of the (ω, p) coupling, therefore it is better to look at how accurate the final solution, obtained from solving (27b) and (30) or (31), will be. When no exact solution or benchmark numerical solution is available, the judgment is difficult to make. However, we may at least infer how well the decoupled methods approximate the global (ω, p) coupling by checking the velocity no-slip condition (since this is the reason for all the trouble). This check cannot be easily done analytically[25] and numerical experiments are needed in many cases.

To gain some insight to the above decoupled approaches, we need to clarify the hidden assumptions of the approximate BCs, especially (31). The common argument that leads to (31) has been reviewed by Gresho.[1] A more rational analysis is as follows.

For the sake of simplicity we consider a two-dimensional flow over a solid surface $y = 0$, with x and y being the tangential and normal directions of the surface respectively. The flow occurs at $y > 0$. For the tangential velocity u at the surface we have

$$\frac{\partial u}{\partial t} + P = -\nu\frac{\partial \omega}{\partial y}, \tag{32}$$

where $P \equiv \partial p_{2B}/\partial x$. Assume initially there is a slip velocity u_s at $y = 0$. Integrating (32) from zero to Δt yields

$$u(\Delta t) - u_s = \Delta t(\bar{\sigma} - \bar{P}), \tag{33}$$

where

$$\bar{\sigma} = \frac{1}{\Delta t}\int_0^{\Delta t} \nu\frac{\partial \omega}{\partial y}\,\mathrm{d}t \quad \text{and} \quad \bar{P} = \frac{1}{\Delta t}\int_0^{\Delta t} P\,\mathrm{d}t$$

are the averaged boundary vorticity flux and pressure gradients respectively. Since the diffusion substep should make the no-slip condition satisfied at $t = \Delta t$, we have

$$\bar{\sigma} = -\frac{u_s}{\Delta t} + \bar{P}. \tag{34}$$

Here $\bar{P}$ is unknown, and by dropping it, we return to the decoupled approximate expression (31) for the averaged vorticity flux. Since u_s represents the initial singularity, $\bar{P}$ should give the 'regular part' of σ, like that in (17a), and can be solved from (29). This implies that as $\Delta t \to 0$,

$$\int_0^{\Delta t} \sigma \, \mathrm{d}t = -u_s, \tag{35}$$

from which we may get $\bar{\sigma} = -u_s/\Delta t$ too; moreover, the derivation seems to suggest that dropping $\bar{P}$ will introduce an $O(\Delta t)$ error. We note that KLP obtained (35) via a different approach. First they obtained an integral equality (for two-dimensional problems), which in our notation reads

$$\int_0^{\Delta t} \oint \sigma \, \mathrm{d}s = -\oint u_s \, \mathrm{d}s,$$

where the closed line integral is along the surface of a solid body. Then follows their key step: equation (35) is *sufficient* for the integral equality to be satisfied. Note that adding a tangential gradient of a single-valued scalar function on the right-hand side of (35) would also ensure the above equality. Comparing with (32) or (33), the scalar function can be identified as the pressure. Therefore the use of (32) avoids such ambiguity and clearly reveals the coupling with the pressure.

To evaluate the accuracy of the decoupled approximation, it suffices to compare $\bar{P}$ with $u_s/\Delta t$. Assume that $\mathbf{u}_0$ satisfies the no-slip condition, so that after the inviscid convection substep we have $u_s = O(\Delta t)$ and hence $u_s/\Delta t = O(1)$. On the other hand, by (29) and the property of the linear operator acting on p_{2B}, we have $p_{2B} = O(\nu\omega_B)$. For a high-Reynolds-number attached boundary layer $\omega_B = O(\nu^{-1/2})$, so

$$\bar{P} \sim \nu \frac{\partial \omega_B}{\partial x} \sim \nu^{1/2}. \tag{36}$$

Therefore for sufficiently high Re the error due to dropping $\bar{P}$ should be $O(Re^{-1/2})$, which is much smaller than $u_s/\Delta t$. In (36) we have assumed that ω_B varies smoothly along the body surface such that $\partial\omega_B/\partial x = O(\omega_B)$. This is not the case for complicated separating flows, since near separation as well as the front stagnation point the tangential gradient of ω_B may be much larger. By the triple-deck theory the streamwise length scale near separation is $\nu^{3/8}$. Thus $\partial\omega_B/\partial x \sim \nu^{-7/8}$ and $\bar{P} \sim \nu^{1/8} \gg \nu^{1/2}$. In this case dropping $\bar{P}$ might be locally unsatisfactory, although it is still asymptotically small as $Re \to \infty$. On the other hand, (36) may still be an effective overall estimate, at least for smoothly separated flows; our numerical tests (Section 4.2) support this conclusion.

Similarly, for three-dimensional flows the extra term in $\boldsymbol{\sigma}$, i.e. $(\mathbf{n} \times \nabla) \cdot (\nu\boldsymbol{\omega}_B \times \mathbf{nn})$, is also small in general. This term involves the possible sharp curvature of the body surface and the critical point behaviour of skin friction lines; see Reference 10 for detailed analysis.

Overall we conclude that (31) is a good approximation when the Reynolds number of the flow is sufficiently high. In any case, owing to ignoring the effect of $\bar{P}$, there will be a residual slip on the boundary even after diffusion.

If the assumption of local unidirectional flow is valid (e.g. Δt is small and the surface is smooth, etc.) and h is taken to be proportional to $\sqrt{(\nu\Delta t)}$, then (30) may give results close to those given by (31). However, carrying the accuracy analysis of (30) further is difficult, solely because of the lack of a local equation for ω_B. Moreover, the arbitrariness of h is an undesirable feature for both theoretical analysis and numerical computation. Again the error will show up in the form of slip.

We end this section with the following comments. First, the above analysis indeed indicates that p_2 is not the pressure solution of the Navier–Stokes equation. In fact, at a high Reynolds number p_2 is only a small part of the pressure, associated with diffusion. In contrast, p_1, the driving force for convection, is dominant. Indeed, from (26a) we have $p_{1B} = O(1)$. In fractional step schemes the effect of this pressure is already reflected by the $O(\Delta t)$-order $\mathbf{u}_s$ after the convection.

Second, there is a general trend of the coupling strength between ω and p. By 'strength' we mean a quantitative measure of the relative importance of the decoupling. The weaker the coupling, the better is the decoupled approximation. Therefore, under the setting of fractional step methods we can conveniently define the coupling strength as the ratio between p_2 and p_1, which leads naturally to the Reynolds number dependence. Our analysis then shows that *the strength of the coupling decreases approximately as* $Re^{-1/2}$. The strongest coupling occurs when $Re \ll 1$: in a two-dimensional steady Stokes flow the relation between p and $\nu\omega$ is simply that of the real and imaginary parts of an analytical function. On the other hand, for the attached boundary layer approximation with $Re \gg 1$ the coupling disappears, since p is given. However, when separation occurs, the coupling must exist. Note that the decoupled approximation discussed here is different from the parabolic boundary layer approximation; when separation occurs, the former only becomes less accurate but the latter breaks down owing to the Goldstain singularity.

Third, the slip due to the decoupled approximation does not accumulate during time marching. Obviously, any slip left by a diffusion substep will be carried over to the initial condition for the diffusion substep in the next time step. Thus, if at the end of a time step the vorticity is under- or overcreated, it will somehow be automatically corrected at the next time step. This self-adjusting feature is common to the above decoupled approximations. However, the ability of self-adjustment varies among different schemes, as will be shown by the numerical examples in the next section.

3. ELEMENTARY NUMERICAL TESTS

To justify the general theory developed in Section 2, both integral and finite difference schemes were tested, with different boundary conditions for vorticity, against some known exact solutions. The selected test cases are (1) an impulsively started rotating circular cylinder, i.e. a generalized Stokes first problem with known exact solution,[26] and (2) a circular cylinder performing rotatory oscillation with an impulsive start, i.e. a generalized Stokes second problem including a transient period, whose exact solution is known[18] only for the steady state ($t \to \infty$). The unidirectional counterparts of these problems have been mentioned in Section 2.2. The flows are rotationally symmetric, so the non-linear convection and the coupling with the tangential pressure gradient are both absent and the processes are purely diffusive. Because the vorticity creation and dynamic vorticity conditions are exclusively governed by diffusion, as indicated by the definition of boundary vorticity flux, these pure shearing motions serve our purpose properly.

3.1. *Integral method and smoothed heat kernel*

For the above generalized Stokes first and second problems the basic integral formula is the purely diffusive version of (14),

$$\omega(t) = 2\oint_B G_0^* \gamma_0 \, dS + \int_V \hat{G}_0^* \omega_0 \, dV + 2\int_0^t d\tau \oint_B G^* \sigma \, dS, \tag{37}$$

where $\hat{G}_0^*$ is G^* plus its image with respect to the cylinder and can be obtained by the same method as the Coulombic kernel. Here the flux σ is exactly known: for the first problem $\sigma = 0$ for $t > 0$; for the second problem $\sigma = \partial b/\partial t = -\sin t$ (we assume $b = \cos t$ so that there is an impulsive start). Thus our task was merely to improve the accuracy of numerical integration, which was carried out by the repeated use of (37) in each time step Δt. After the first Δt the volume integral in (37) is no longer zero, which becomes the most time-consuming part. Therefore a six-point Gaussian quadrature formula was used for surface integrals, while the volume integral was first done by simple summation.

To perform the integration in a polar co-ordinate system (r, θ), a grid with equal size in the θ-direction was used. For the radial direction we set $z = \log r$ and divide the z-interval equally so that the resulting grid is more clustered near the boundary to help resolve the large vorticity gradient there. Owing to symmetry, the main factor influencing the accuracy is Δz, the grid size in the z-direction. In all test cases presented in this subsection, $\Delta t = 0{\cdot}02$ was used. The solution for the Stokes first problem is shown in Figure 1 with $Re = 1000$ and $\Delta z = 0{\cdot}00084$. Note that the error near the boundary is rather significant, which is mainly due to the inaccurate volume integral.

Two methods can be used to improve the accuracy. One is a higher-order volume integration method, such as Gaussian quadrature, and the other is a smoothed kernel method. We chose the latter because it is simple to implement. More importantly, it is generally applicable to the deterministic diffusion part of a vortex method. Thus we replace G^* by a smoothed kernel G_δ^*,

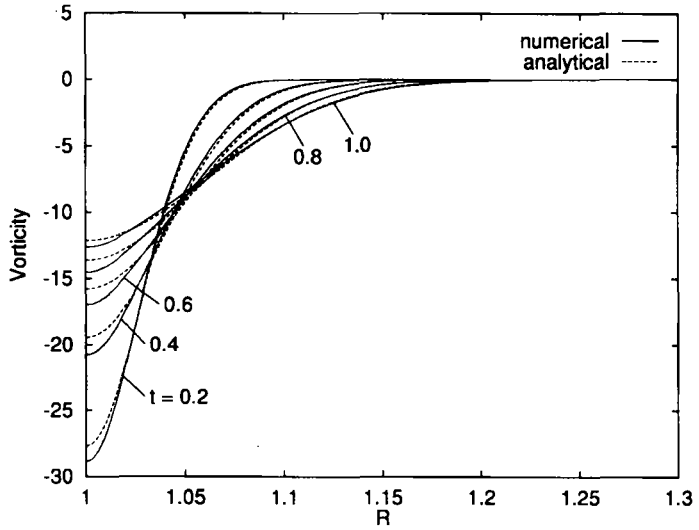

Figure 1. Solution of generalized Stokes first problem using non-smoothed kernel with $\Delta z = 0{\cdot}00084$

even though in computations G^* did not show any singularity. The technique is borrowed from that for the Coulombic kernel G defined by (23), which has been successfully applied in vortex methods. A smoothing function can be taken as

$$\psi(\delta) = \frac{1}{\pi\delta^2} e^{-r^2/\delta^2}. \tag{38}$$

After some straightforward algebra involving special functions, the convolution of $\psi(\delta)$ with G^* gives

$$G_\delta^{*(2)} = \frac{1}{\pi(a^2 + \delta^2)} \exp\left(-\frac{r^2}{a^2 + \delta^2}\right), \qquad a^2 \equiv 4\nu t, \tag{39}$$

where the index (2) implies that this is a second-order kernel. Beale and Majda[27] showed that proper linear combinations of functions like (38) can be used to construct higher-order smoothed Coulombic kernels, and their results can well be applied to heat kernels. For instance, the sixth-order smoothing function found by Beale and Majda is

$$\psi(\delta) = \frac{1}{\pi\delta^2}\left(\frac{8e^{-r^2/\delta^2}}{3} - e^{-r^2/2\delta^2} + \frac{e^{-r^2/4\delta^2}}{12}\right),$$

from which we obtain

$$G_\delta^{*(6)} = \frac{8}{3\pi(a^2 + \delta^2)} \exp\left(-\frac{r^2}{a^2 + \delta^2}\right) - \frac{2}{\pi(a^2 + 2\delta^2)} \exp\left(-\frac{r^2}{a^2 + 2\delta^2}\right) + \frac{1}{3\pi(a^2 + 4\delta^2)} \exp\left(-\frac{r^2}{a^2 + 4\delta^2}\right). \tag{40}$$

The result for $G_\delta^{*(6)}$ with $\Delta z = 0{\cdot}0034$ and $\delta = 2.5\Delta z$ is shown in Figure 2, where the agreement with the exact solution is excellent.

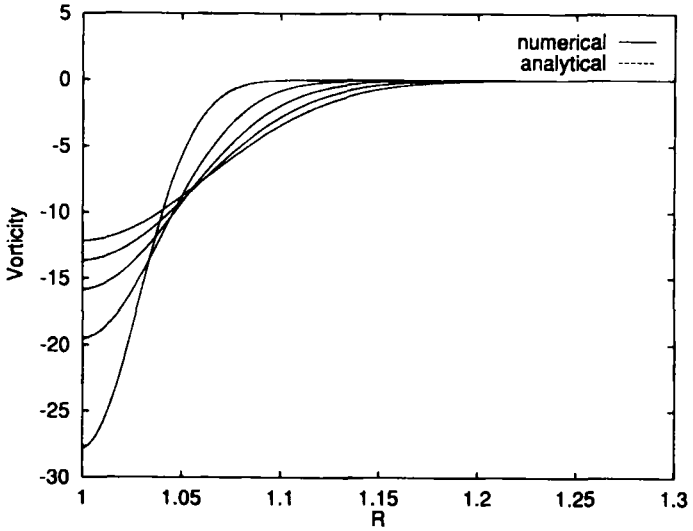

Figure 2. Solution of generalized Stokes first problem using sixth-order smoothed kernel with $\Delta z = 0{\cdot}0034$; for time sequence see Figure 1

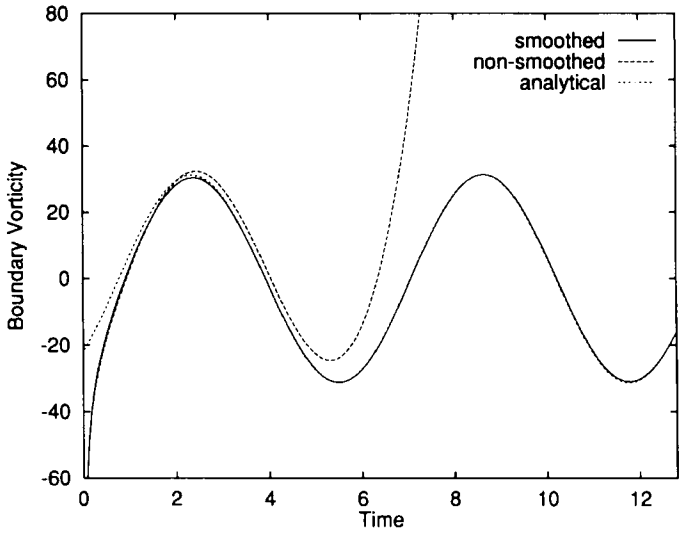

Figure 3. Solution of boundary vorticity of Stokes second problem using sixth-order kernel ($\Delta z = 0{\cdot}0034$) and non-smoothed kernel ($\Delta z = 0{\cdot}00084$) compared with steady state analytical solution

Both non-smoothed and smoothed kernels were used to compute the Stokes second problem with $Re = 1000$. Figure 3 shows the time variation of boundary vorticity using $G_\delta^{*(6)}$ with $\delta = 2{\cdot}0\Delta z$ and the non-smoothed kernel. The grid sizes are the same as above for the two kernels respectively. The short-dashed curve is the analytical steady state solution ($t \to \infty$) and the solid curve is the solution using the smoothed kernel which contains the transient part. The agreement in the smoothed kernel case is again very good. However, using direct summation of the non-smoothed kernel made the scheme blow up after the first period of oscillation (see dashed curve). Although the reason is not totally clear at the moment, we observe that with the smoothed kernel the scheme is not only more accurate but also more stable.

It is evident that if we set $\delta^2 = 4\nu\delta t$, then the smoothed heat kernels will have a simple interpretation: the diffusion process is numerically moved forwards by δt (which has no direct relation with the computation time step Δt). In particular, (39) simply becomes

$$G_\delta^{*(2)} = \frac{1}{4\pi\nu(t+\delta t)} \exp\left(-\frac{r^2}{4\nu(t+\delta t)}\right);$$

thus at $t = 0$

$$G_{\delta 0}^{*(2)} = \frac{1}{4\pi\nu\delta t} \exp\left(-\frac{r^2}{4\nu\delta t}\right),$$

which is regular even for $r = 0$. This implies that the singular initial condition of vorticity is smoothed out. The application of this idea to finite difference schemes was tested numerically for the above problems by Wu.[28] AR also studied the smoothed initial condition and found that it is of crucial importance for the finite difference scheme to have high-order accuracy.

Finally, a fast summation algorithm for heat kernels, of great value in integral methods, has been developed by Greengard and Strain.[29] Based on the same principle, KLP successfully developed and applied a fast deterministic diffusion scheme for the vortex methods.

3.2. Finite difference tests

Because numerical quadratures are time-consuming, a finite difference method was also tested for the generalized Stokes problems. Note that since p is decoupled from ω owing to symmetry, equation (31) is now an exact expression if σ is the averaged flux, but (30) is not. In the following we show how to use (31) to obtain a highly accurate scheme and we present a comparison among the schemes with different vorticity boundary conditions on the cylinder surface.

In the polar co-ordinate system (r, θ), after the transformation $z = \log r$, the vorticity equation for the present case reads

$$r^2 \frac{\partial \omega}{\partial t} = \frac{1}{Re} \frac{\partial^2 \omega}{\partial z^2}, \tag{41}$$

with $\omega = 0$ as $r \to \infty$. Introducing a streamfunction (which is not necessary here, but serves to mimic the general 2D situation), we have

$$\frac{\partial^2 \psi}{\partial z^2} = -r^2 \omega, \qquad -\frac{\partial \psi}{\partial z} = ru, \tag{42a}$$

where u is the velocity along the θ-direction. The boundary conditions are

$$\psi(0, t) = 0, \qquad -\frac{\partial \psi}{\partial z}(0, t) = v(0, t) = b(t), \qquad \frac{\partial \psi}{\partial z}(0, z) = 0 \quad (\text{as } z \to \infty). \tag{42b}$$

In our test equation (41) was discretized using the Crank–Nicolson scheme and all spatial derivatives were discretized via central difference. Note that the velocity on the cylinder surface, u_B, is computed by

$$u_B = -\frac{\psi_1}{\Delta z} - \frac{\Delta z}{2} \omega_B, \tag{43}$$

where $\psi_1 = \psi(\Delta z)$. From (43) we can derive the first kinematic boundary condition for ω, which has been widely used in more general situations. The no-slip condition implies $u_B = b$ and hence

$$\omega_B = -\frac{2\psi_1}{\Delta z^2} - \frac{2b}{\Delta z}. \tag{44}$$

Care is needed regarding (44). Strictly, we should use

$$\omega_B^{n+1} = -\frac{2\psi_1^{n+1}}{\Delta z^2} - \frac{2b^{n+1}}{\Delta z}, \tag{44'}$$

where $n + 1$ denotes the time step. However, in many cases

$$\omega_B^{n+1} = -\frac{2\psi_1^n}{\Delta z^2} - \frac{2b^n}{\Delta z} \tag{44''}$$

is often used, especially when the solid body is at rest; since its right-hand side contains no unknown quantity, it is truly local, whereas (44') is not. This localized version is called BC1 here. The second boundary condition is the 2D version of (30), BC2. Both BC1 and BC2 are Dirichlet conditions and are easy to implement. In fact, under certain conditions these two versions are identical.[30]

The third boundary condition, BC3, is (34) where P is absent. BC3 is of the Neumann type and can be discretized in various ways. Meanwhile, there are also several ways to compute u_B or u_s. It should be emphasized that one has to choose the methods consistently. This subtle issue is being studied and will be reported separately. For the present cases one consistent approach is to apply the Crank–Nicolson discretization at the nodal point 0 and take

$$\omega_1 - \omega_{-1} = -2\Delta z \frac{\sigma}{\nu}$$

into account. This yields

$$(1 + 2\lambda)\omega_B^{n+1} - 2\lambda\omega_1^{n+1} = (1 - 2\lambda)\omega_B^n + 2\lambda\omega_1^n \frac{2u_s}{\Delta z}, \tag{45}$$

where $\lambda = \nu\Delta t/2\Delta z^2$. The last terms on the right-hand side of (45) is nothing but what Anderson[7] proved to be the 'induced' vorticity on the boundary by u_s, though his result was obtained for boundary layer flow and from a different approach:

$$\omega_B^{n+1} - \omega_B^n = -\frac{2u_s}{\Delta z}. \tag{46}$$

Thus the interconnection between the dynamic condition and its kinematic counterpart is rediscovered. Equation (45) uses the assumption $\bar{\sigma} = \frac{1}{2}(\sigma^n + \sigma^{n+1})$ and is thus $O(\Delta t^2)$-accurate, in contrast with the $O(\Delta t)$-accuracy of BC1 and BC2.[30] Furthermore, the dynamic feature as reflected by λ is preserved in (45) but lost in (46), which, as we shall see, makes an important difference in the stability of the schemes.

Figure 4 shows the results for the first Stokes problem ($\Delta z = 0{\cdot}0067$, $\Delta t = 0{\cdot}02$). From the comparison of the variation in ω_B and u_s versus time, it is seen that the scheme with BC3 adjusts itself quickest to the correct path of solution. In fact, when BC3 was used, after the first time step the slip was immediately reduced to 10^{-7}. In contrast, the slip of the other two schemes reduced gradually; at the end of 100 time steps it was about 10^{-4}. Therefore BC3 is the best in achieving the no-slip constraint, since physically $\boldsymbol{\sigma}$ and $\mathbf{u}_s$ are directly and locally related. However, the vorticity solution of BC3, especially near the boundary and when t is small, is less accurate than the other two, as shown by Figure 4(a). We merely point out here that the method of computing slip is only second-order. Thus it cannot give an accurate measure of slip shortly after the impulsive start when the vorticity gradient is very large. This observation poses a design problem for the schemes that really need to achieve the no-slip condition. One solution is to construct higher-order methods.[8]

The numerical oscillation in Figure 4(b) reveals a more serious problem with BC1 and BC2 than it appears. The oscillations are caused solely by the inconsistencies between kinematic boundary conditions and the dynamics. For example, in (44) the boundary condition varies with Δz instead of Δt, meaning that ω_B is the same no matter how large the first time step is. When the error is too large, the scheme cannot recover from oscillation and blows up. This situation is similar for BC2. However, if h takes the form of $C\sqrt{(\nu\Delta t)}$, where C is a constant, the scheme is unlikely to break down, because the dynamics are partially reflected (in a rather approximate way). However, longer-time oscillations occur before the result converges. The oscillation and possible instability problem is most severe for impulsively started flows where the initial slip is

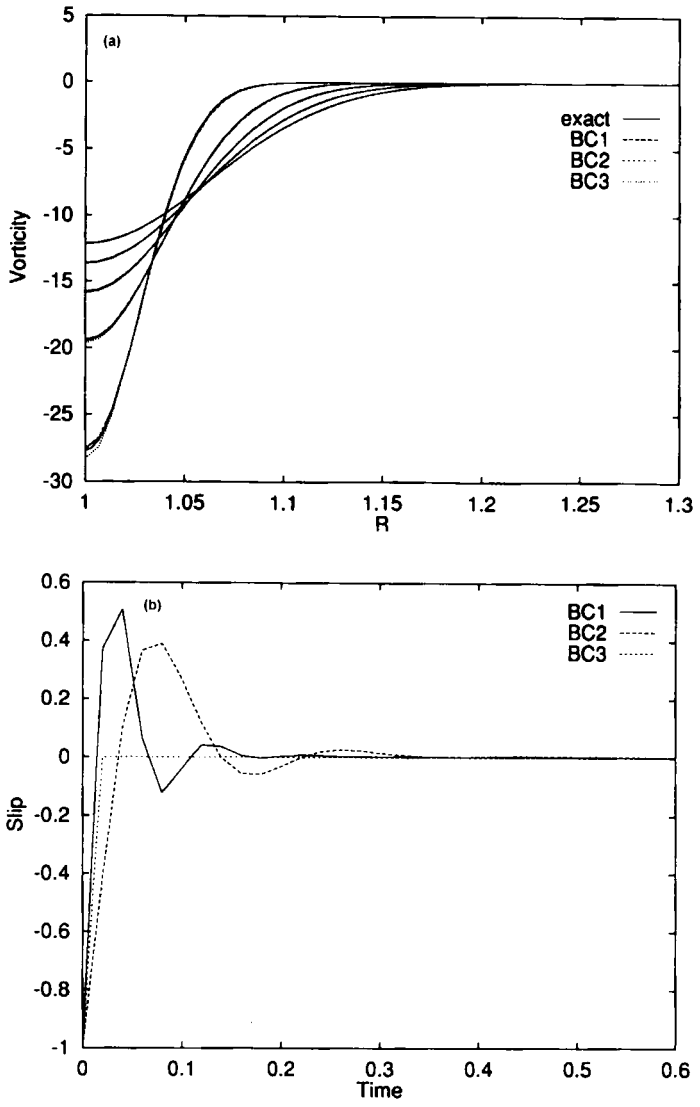

Figure 4. Finite difference solutions of Stokes first problem with different numerical boundary conditions for vorticity ($\Delta z = 0{\cdot}0067$, $\Delta t = 0{\cdot}02$): (a) vorticity distribution at different times (see Figure 1); (b) time variation of slip

very large. More analysis of the advantages of the Neumann condition over Dirichlet ones are given by Wu.[30]

The Stokes second problem is also solved by using the above three boundary conditions. The comparison is shown in Figure 5. Essentially no new difficulties occur, except that the slip using BC1 and BC2 increases. In the computation $b(t) = \cos t$ was used intentionally to provide the impulsive start, which is our main interest here. One could avoid the transient part of the solution by using the steady state result (after one period of rotation) as the initial condition.

Finally, we note that using (44′) is equivalent to imposing $u_s^{n+1} = 0$. Since using BC3 also achieves this condition, the two BCs should give the same solution because of uniqueness.

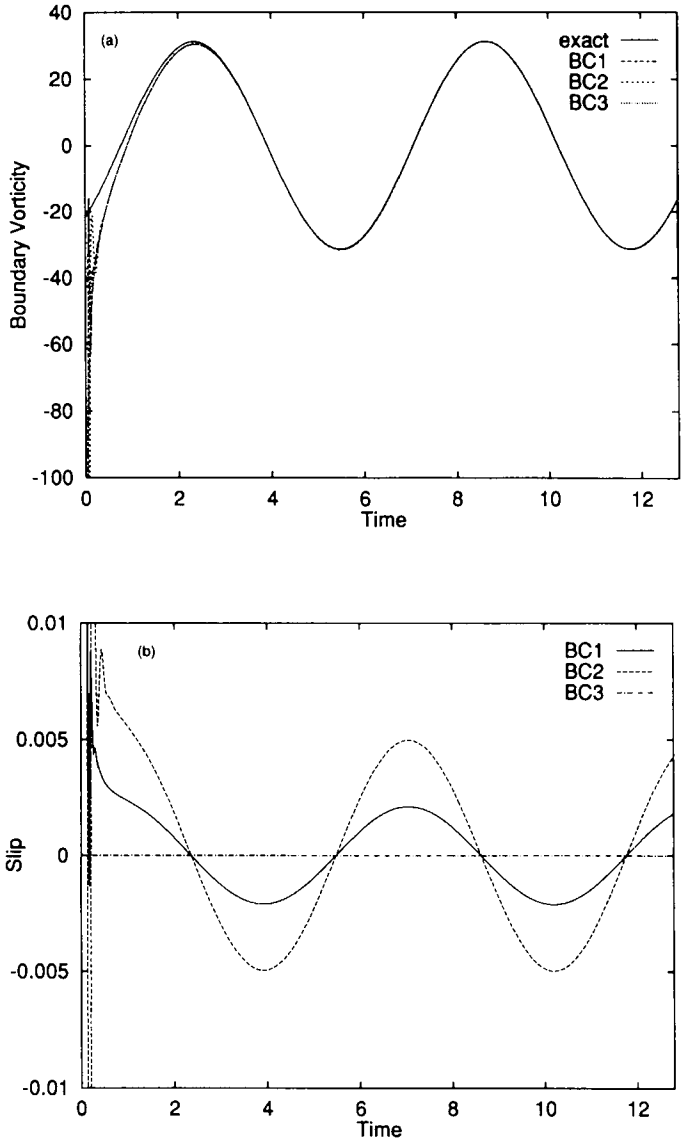

Figure 5. Finite difference solution of Stokes second problem with different numerical boundary conditions for vorticity (with same parameters as Figure 4): (a) time variation of boundary vorticity; (b) time variation of slip

4. IMPULSIVELY STARTED FLOW OVER CIRCULATION CYLINDER

We now turn to the general situation at high Reynolds numbers, where the coupling with pressure appears but the decoupled approximation is feasible. We examine how the decoupled scheme works and how to recover the global coupling through an efficient iterative scheme. The results are compared with the experiments of Bouard and Coutaneau[31] and the highly accurate computation of AR. That accurate computation used an explicit fourth-order Runge–Kutta scheme in time with fourth-order central difference in space, a fully coupled treatment of the

vorticity boundary condition (equivalent to the discretized version of the integral–differential equation derived by Anderson[7]) and a domain decomposition method to accurately reflect the infinite boundary conditions. The comparison further confirms our theoretical analysis.

4.1. Formulation and numerical scheme

The test case is a circular cylinder with radius R in a cross-flow with freestream speed U. The Reynolds number is $Re = 2UR/\nu$. Using U and R to non-dimensionalize the vorticity and streamfunction equations yields

$$A\frac{\partial\omega}{\partial t} + \frac{\partial}{\partial z}\left(\frac{\partial\psi}{\partial\theta}\omega\right) + \frac{\partial}{\partial\theta}\left(-\frac{\partial\psi}{\partial z}\omega\right) = \frac{2}{Re}\left(C\frac{\partial^2\omega}{\partial z^2} + B\frac{\partial\omega}{\partial z} + \frac{1}{C}\frac{\partial^2\omega}{\partial\theta^2}\right), \tag{47a}$$

$$C\frac{\partial^2\psi}{\partial z^2} + B\frac{\partial\psi}{\partial z} + \frac{1}{C}\frac{\partial^2\psi}{\partial\theta^2} = -A\omega, \tag{47b}$$

where

$$z = \log(r + a), \qquad A = e^z(e^z - a), \qquad B = ae^{-z}, \qquad C = 1 - ae^{-z} \tag{47c}$$

and a is a strain parameter to make the grid more clustered near the cylinder surface. We use the potential flow solution as the initial condition, in which the normal velocity condition is imposed by letting $\psi = 0$ at the solid boundary.

Because of the periodicity in the θ-direciton, equation (47b) can be solved by using FFT in the θ-direction and solving the tridiagonal system of equations (due to central difference discretization) in the z-direction. Once ψ is known, the velocity is obtained by taking the central difference of ψ. The resulting scheme is fast and second-order-accurate.

For (47a) we use fractional step methods. Both the first-order scheme

$$\mathbf{u}^n = (H(\Delta t)E(\Delta t))^n\mathbf{u}^0 \tag{48}$$

and the second-order scheme (Strang splitting)

$$\mathbf{u}^n = (H(\Delta t/2)E(\Delta t)H(\Delta t/2))^n\mathbf{u}^0 \tag{49}$$

were tested. Note that (49) is only a little more expensive than (48), as can be seen by rewriting it as

$$\mathbf{u}^n = H(\Delta t/2)(E(\Delta t)H(\Delta t))^{n-1}E(\Delta t)H(\Delta t/2)\mathbf{u}^0. \tag{49'}$$

Thus extra cost occurs only when the output of intermediate values is desired.

For the convection operator $E(\Delta t)$ we combine QUICK upwind differencing,[32] which does not suffer from second-order numerical diffusion, and second-order TVD Runge–Kutta time discretization.[33] The scheme was tested against a one-dimensional linear problem (see Reference 33 for details) and compared with a third-order ENO scheme (Figure 6). Although an oscillation does appear in the results of QUICK differencing, it does not cause serious trouble, because the flow is incompressible and viscous. Besides, the oscillation is much less severe than that coming from using second-order central difference, and the scheme is much faster than the ENO scheme.

The diffusion operator $H(\Delta t)$ is the focus of the present study, which by (47) reads

$$A\frac{\partial\omega}{\partial t} = \frac{2}{Re}\left(C\frac{\partial^2\omega}{\partial z^2} + B\frac{\partial\omega}{\partial z} + \frac{1}{C}\frac{\partial^2\omega}{\partial\theta^2}\right). \tag{50}$$

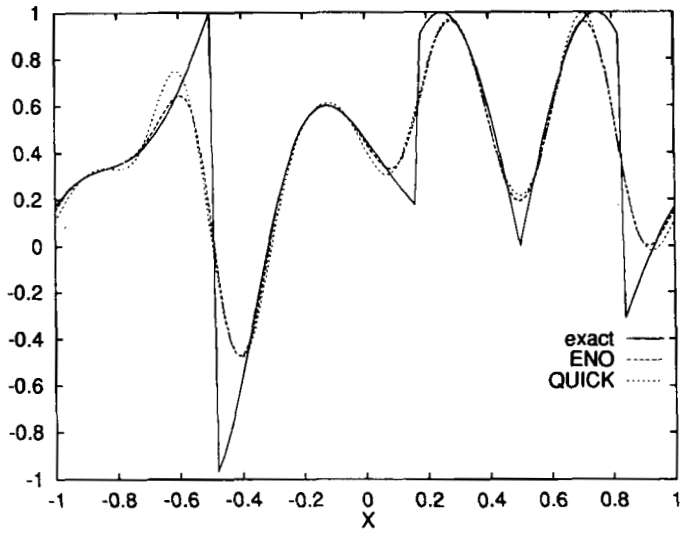

Figure 6. Comparison between third-order ENO and QUICK schemes using 1D linear convection equation

At the cylinder surface we have

$$\frac{\partial u}{\partial t} = -e^z \frac{\partial p}{\partial \theta} + \frac{2}{Re} \frac{\partial \omega}{\partial z}, \tag{51}$$

where $u = -\partial\psi/\partial z$. Let

$$P = e^z \frac{\partial p}{\partial \theta}, \qquad \sigma = -\frac{2}{Re} \frac{\partial \omega}{\partial z}.$$

Integrating (51) gives

$$\frac{u^{n+1} - u^{n+1/2}}{\Delta t} = -\bar{P} - \bar{\sigma}, \tag{52}$$

where $n + \frac{1}{2}$ denotes the values after $E(\Delta t)$. Imposing the no-slip condition at the $(n + 1)$th step yields

$$\bar{\sigma} = \frac{u^{n+1/2} - b^{n+1}}{\Delta t} - \bar{P}. \tag{53}$$

Now we integrate (50) with respect to t and obtain

$$A(\omega^{n+1} - \omega^{n+1/2}) = \frac{2\Delta t}{Re}\left(C \frac{\partial^2 \bar{\omega}}{\partial z^2} + B \frac{\partial \bar{\omega}}{\partial z} + \frac{1}{C} \frac{\partial^2 \bar{\omega}}{\partial \theta^2}\right), \tag{54}$$

where $\bar{\omega}$ is the time-averaged value of ω. Note that by applying (54) at the boundary, we can incorporate the dynamic condition (53) into the scheme without approximating $\bar{\sigma}$. Moreover, the Crank–Nicolson scheme follows from the approximation

$$\bar{\omega} = \tfrac{1}{2}(\omega^{n+1} + \omega^{n+1/2}). \tag{55}$$

Equations (54) and (55) can be solved efficiently by approximate factorization. We use the Peaceman–Rachford ADI scheme and discretize the spatial derivative, including the boundary terms, by central difference. Thus the resulting systems of equations are tridiagonal. To close the equations, we need to know $\sigma^{n+1/2}$ and σ^{n+1}. It is evident from the discussion about (54) that only $\bar{\sigma}$ is important in the unfactored scheme. Therefore, as long as $\bar{\sigma} = (\sigma^{n+1/2} + \sigma^{n+1})/2$ is satisfied, no matter how we choose the two values, the scheme should be consistent. Thus we simply set $\sigma^{n+1/2} = \sigma^{n+1} = \bar{\sigma}$.

As shown in Section 2, dropping $\bar{P}$ introduces some error into the solution and the no-slip condition is not strictly satisfied. Although the error is generally not large, as an unknown factor is it undesirable for designing highly accurate numerical schemes. Thus we introduce an iterative method that controls the slip to a desired small level, i.e. we *bypass solving pressure but retain the global* (ω, p) *coupling by iteration.* If the initial guess is close to the solution, the iteration technique is more efficient compared with directly imposing the global coupling. This is the case here because of the high Reynolds number.

The iterative scheme can be naturally derived from (52) and (53). Initially we drop $\bar{P}$ and get

$$\bar{\sigma}^0 = \frac{u^{n+1/2} - b^{n+1}}{\Delta t}. \tag{56}$$

For a fully decoupled scheme equation (56) is the boundary condition to use. After the diffusion $u^{n+1,0} \neq b^{n+1}$ in general. Thus subtracting (56) from (52) gives

$$\bar{P}^0 = -\frac{u^{n+1,0} - b^{n+1}}{\Delta t} = -\frac{u_s^{n+1,0}}{\Delta t}.$$

Substituting this result into (53), we obtain an updated boundary condition

$$\bar{\sigma}^1 = \bar{\sigma}^0 + \frac{u_s^{n+1,0}}{\Delta t}$$

and hence in general

$$\bar{\sigma}^{m+1} = \bar{\sigma}^m + \frac{u_s^{n+1,m}}{\Delta t}. \tag{57}$$

Clearly, (57) converges when the no-slip condition is achieved.

Note that during the iteration only the slip needs to be computed. This feature makes (57) fit well in a vortex method that solves velocity via the Biot–Savart integration, because the slip can be obtained without solving the whole velocity field. However, for the current finite difference method we still have to solve the whole field. Since the Poisson solver is fast and the iteration converges fast, as will be seen below, our scheme is still reasonably fast.

An advantage of the present fractional step method is that we can use Δt larger than that allowed by the CFL number of the explicit convection scheme. Since the convection and diffusion are performed in turn and the diffusion scheme is unconditionally stable, we can perform several convection substeps with a smaller Δt that satisfies the CFL condition, and one diffusion step with a larger Δt. Obviously, by doing this, we can save CPU time while getting the same result if Δt is not too large to degrade the time accuracy. This is especially useful when a tiny grid size has to be used for computing high-Reynolds-number flows.

As to the far-field boundary condition, in the present computation we impose the potential flow solution of ψ at r_∞, which is commonly done in this type of computation. For the vorticity

we convect ω out of the computational domain by upwind differencing. The value of ω at r_∞ is then used as the boundary condition for the diffusion substep.

4.2. *Results and discussion*

Both the first- and second-order splitting schemes were used to compute the impulsively started flow with $Re = 9500$. At this Reynolds number the flow exhibits a rich vortex structure which makes the computation difficult. In the following results the far-field boundary is taken to be $r_\infty = 5$ unless otherwise stated; a 512×301 grid was used, except for Figures 7 and 8 below where the grid was 256×301. The computation was done in double precision on a Sun SPARC10 workstation. With the 256×301 grid it took about 5 CPU seconds for one time step without iteration.

Figure 7 shows the computed flow field using the first-order splitting and no iteration, compared with experiment[31] and the computation by Ta Phuoc Loc and Bouard.[34] The results were obtained with $a = -0{\cdot}5$, so the grid sizes are $\Delta\theta = 0{\cdot}0245$ and $\Delta z = 0{\cdot}0073$, and we have

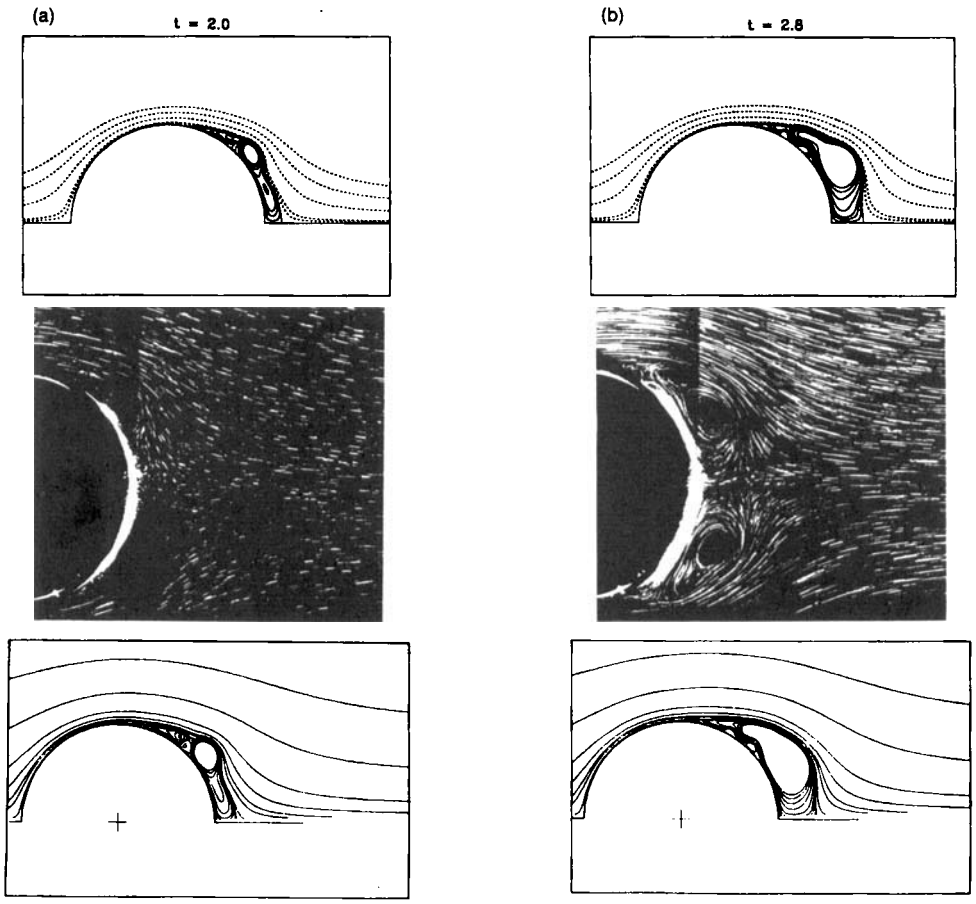

Figure 7. Comparison of flow structure obtained by present fractional step scheme on a 256×301 grid (top; $a = -0{\cdot}5$, $r_\infty = .5$, $\Delta t = 0{\cdot}0005$), flow visualization (middle) and numerical solution simulation of Ta Phuoc Loc and Bouard (bottom): (a) $t = 2{\cdot}0$; (b) $t = 2{\cdot}8$; (c) $t = 3{\cdot}2$; (d) $t = 4{\cdot}0$

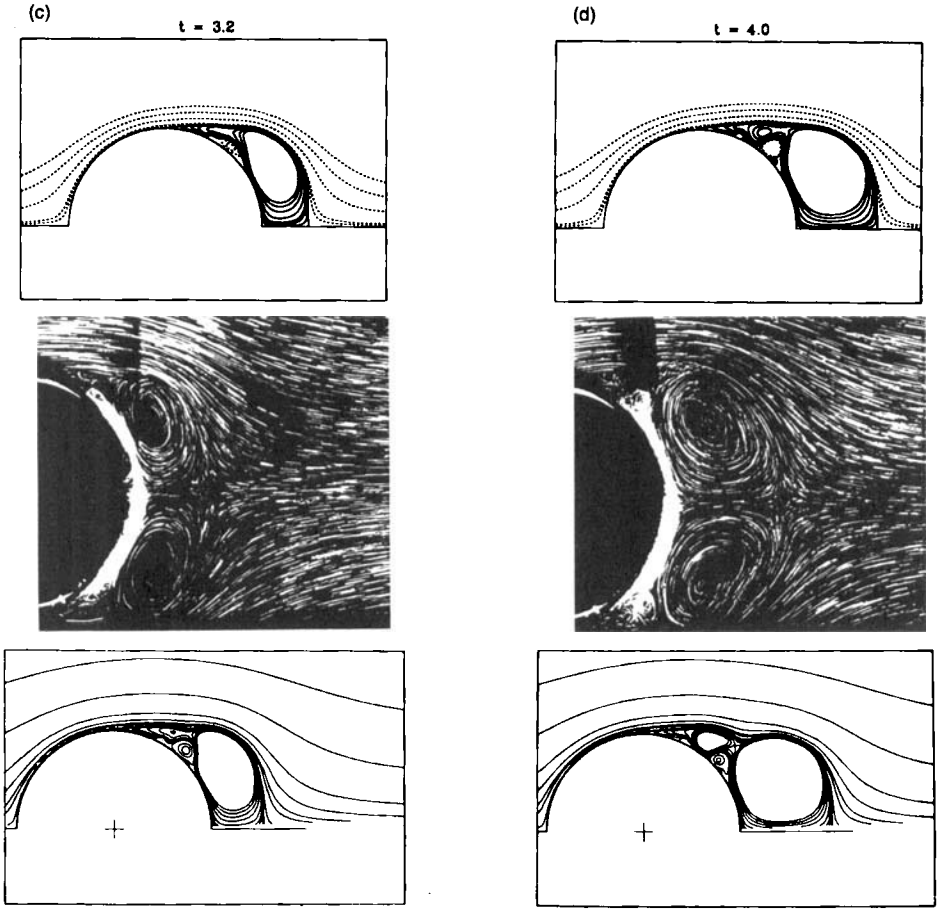

Figure 7 (*continued*)

$\Delta r = 0{\cdot}0037$ adjacent to the wall, which will be denoted by Δr_B. The time step is $\Delta t = 0{\cdot}005$. The agreement is good. It needs to be stressed that such comparison is only of qualitative value. Later we shall compare the results of ω_B and the drag coefficient C_D, which will give more quantitative information about our scheme. In Figure 8 the velocity at the symmetry plane behind the cylinder is compared with experiment. The solid curves are the numerical results and the symbols experimental data. We note that the wake length of our computation is always smaller than that of the experiment[31] as well as Ta Phuoc Loc and Bouard's results (Figure 7). On the other hand, our result agrees well with AR's fourth-order computation (see Figure 14 below). We believe that besides the grid size and r_∞ effect to be discussed below, the different treatment of the initial condition is an important source of the discrepancy with that of Ta Phuoc Loc and Bouard. In both the present and AR's computations a potential flow (with modification in the latter case) was used to model the 'impulsive' start, while an initial Stokes flow with a sudden change in the Reynolds number was used by Ta Phuoc Loc and Bouard.[34]

The comparison in Figure 7 seems to suggest that the flow is well resolved. Indeed, a comparison of ω_B using the above grid with AR's fourth-order solution (obtained on a uniform grid with $\Delta\theta = 0{\cdot}00307$, $\Delta r = 0{\cdot}00195$ and $\Delta t = 0{\cdot}00033$) showed that the attached and smooth

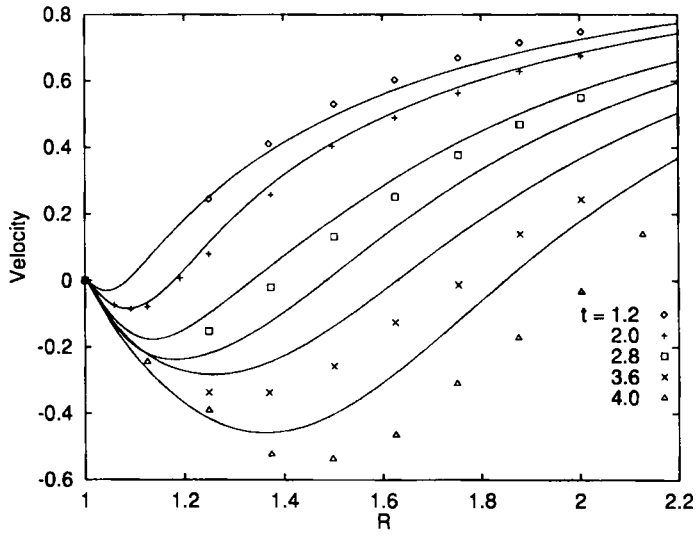

Figure 8. Comparison of wake velocity profile between numerical and experimental results (see Figure 7 for parameters)

separating flows are well resolved with our much larger $\Delta\theta$. However, for resolving the more complicated separating flow, a smaller $\Delta\theta$ is necessary. Thus we reduced $\Delta\theta$ to 0·0123 by increasing the grid number in the θ-direction, n_θ, to 512 (Δt was reduced to 0·0025). The results of ω_B with and without iteration are shown in Figure 9. The agreement is good except for the extreme values.

The time variation of the maximum and averaged slip (under the L_2-norm) is shown in Figure 10. To the author's knowledge, in the literature only Cottet[19] mentioned that in his computation the averaged slip is about 2%. It is interesting to note that after keeping at a constant level (with maximum slip 0·0125%) for some time, the slip rises up. The time of slip rising is about the time when the first secondary vortex starts to form. Owing to these small vortices rather than the primary large vortex, the boundary vorticity no longer varies smoothly along the surface; a large gradient occurs. This can also be seen clearly in Figure 9. Comparing Figure 9(b) with Figure 10 shows that when $t = 2$, there are high peaks in the ω_B distribution (in fact, the maximum boundary vorticity occurs at about this time), so that not only ω_B but also its gradient is large. Correspondingly, the slip is larger, about the maximum point in the curve. This observation is in qualitative agreement with our previous discussion on the accuracy of decoupled schemes.

There are two ways to further improve the accuracy in ω_B. First, when there is a high peak in ω_B, the normal gradient near the wall is likely to be very high. Thus reducing Δr near the wall will give better resolution. The other way is to use the iteration method so that the slip can be further reduced and the global coupling is better satisfied. We need to point out, however, that *the slip does not directly relate to the accuracy of* ω_B, although vorticity is created by the no-slip condition (recall that ω_B is the space–time-integrated effect of σ).

We implemented the iterative scheme and let the averaged slip reduce to below 10^{-6}, which is below the discretization error. Only two or three iterations were needed for convergence. The fast convergence of the iterative scheme is mainly because of the weak coupling as discussed in Section 2. The result (Figure 9) is almost identical with the non-iterative one. This indicates that

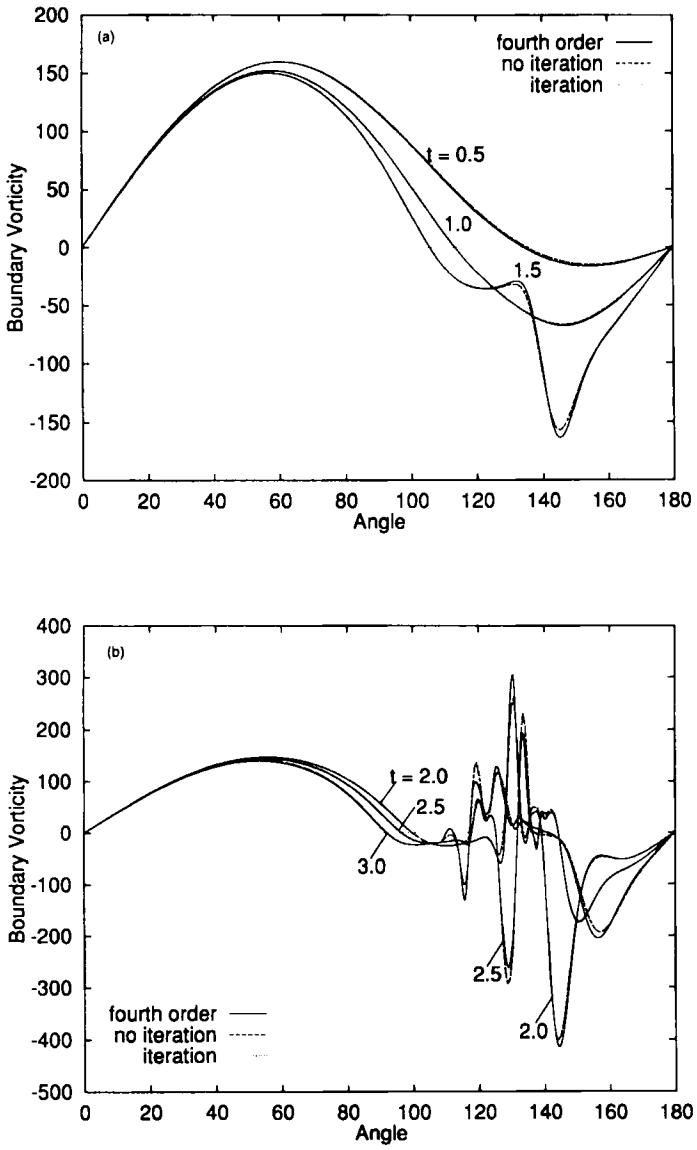

Figure 9. Comparison of boundary vorticity obtained by present scheme on a 512 × 301 grid ($a = -0{\cdot}5$, $r_s = 5$, $\Delta t = 0{\cdot}0025$) and fourth-order scheme of Anderson and Reider

for the present high-Reynolds-number flow the (ω, p) coupling is so weak that the decoupled approximation is good enough, at least in the range of the present second-order accuracy. On the other hand, the second-order method of computing slip might degrade the effectiveness of the iteration. Note that the slip is most influenced by the vorticity distribution near the wall; when large gradients are present in that region, the slip could be difficult to compute accurately even by the second-order method. To make the iteration more beneficial, therefore, higher-order methods might be needed for computing the slip. Examples of these methods, but in different

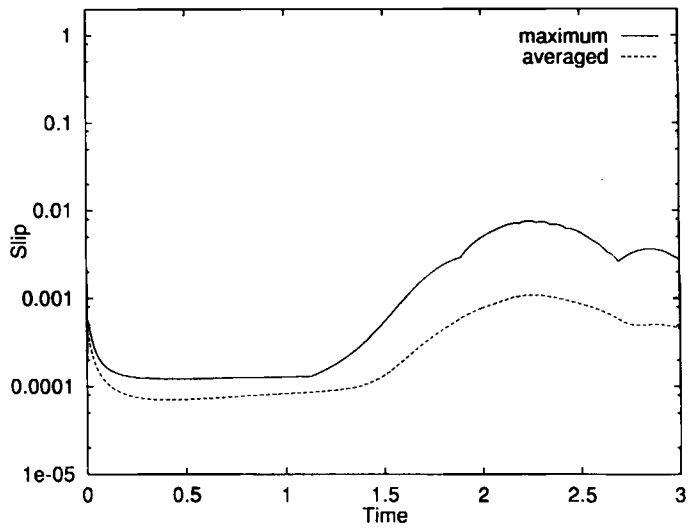

Figure 10. Time variation of maximum and averaged slip velocities (see Figure 9 for parameters)

contexts, include that by Ta Phuoc Loc and Bouard,[34] who used a compact fourth-order scheme to compute the streamfunction and velocity, and that by AR, who tested a hybrid scheme with higher-order computation of both u_s and ω_B.

Now we reduce Δr close to the wall by choosing the strain parameter $a = -0{\cdot}9$ ($\Delta r_B = 0{\cdot}00124$) and use two different Δts, i.e. 0·001 and 0·01. The results for ω_B (without iteration) are shown in Figure 11. Comparing with Figure 9, the improvement in the peak values of ω_B is obvious. The influence of Δt, also shown in the figure, turns out to be small. In fact, we also tested the second-order splitting scheme with the same grid and time steps and obtained little improvement. It seems that the time accuracy is not crucial in the present early-stage computation. Furthermore, the time accuracy of the second-order splitting may be deteriorated by the singular initial condition for vorticity, as AR observed.

Figure 12 shows a comparison of the slip variation with different time steps (no iteration). It clearly indicates that the residual slip after the diffusion substep is proportional to Δt. Recall that the first estimate of $\bar{P}$ is just the ratio of this residual slip to Δt; therefore $\bar{P}$, and hence the error introduced by dropping $\bar{P}$, is *independent* of Δt, which is physically correct. This error should depend mainly on the Reynolds number as discussed in Section 2.3. Similar Δt independence holds for the performance of the iterative method. Comparing the maximum slip in Figure 10 with that obtained with $\Delta t = 0{\cdot}0025$ in Figure 12, we see very similar slip variation. In fact, our numerical experiments showed that the magnitude of slip has little dependence on the grid size.

In order to further confirm the estimate (36), a group of tests were performed with fixed Δt to check the dependence of the residual slip, and hence $\bar{P}$, on Re. We define the reduction factor of the slip by

$$f_R = u_s^{n+1}/u_s^{n+1/2},$$

where $u_s^{n+1/2}$ and u_s^{n+1} are the slip values after the convection and diffusion substeps respectively. Evidently f_R also represents the ratio between p_1 and p_2, or the inverse of the strength of (ω, p)

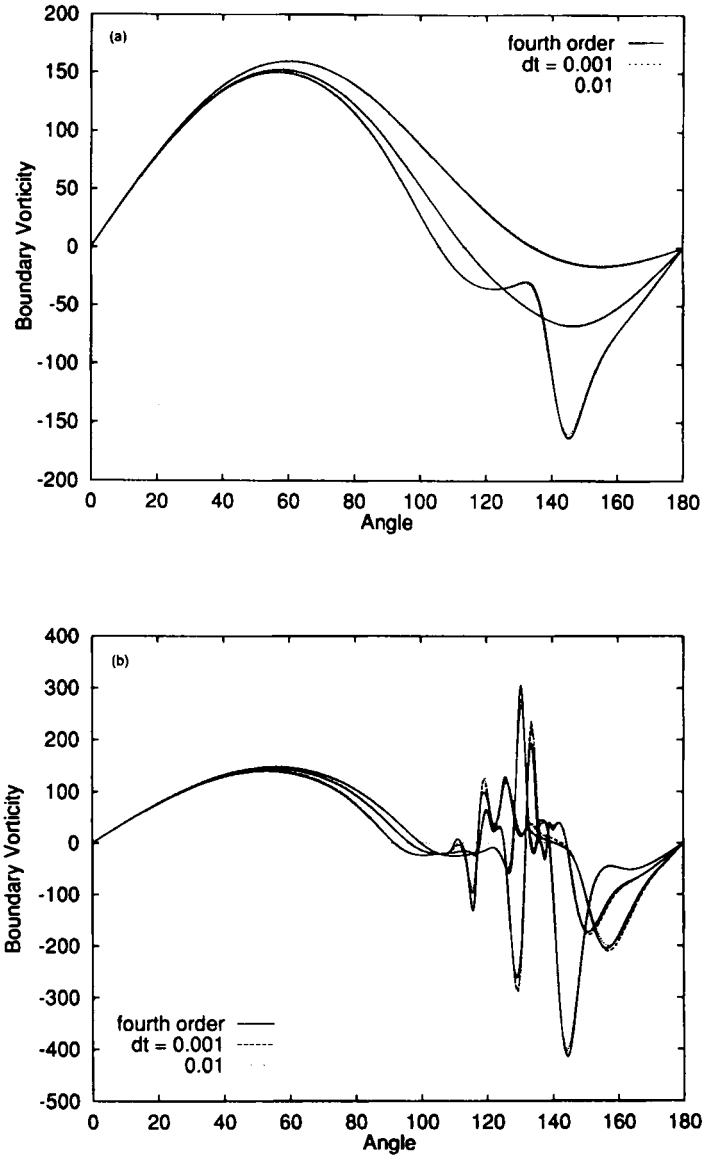

Figure 11. As Figure 9; $a = -0{\cdot}9$ and $\Delta t = 0{\cdot}001, 0{\cdot}01$

coupling. To determine the variation in f_R with Re, we define the index of f_R as

$$I_R = \frac{\ln(f_{R_2}/f_{R_1})}{\ln(Re_2/Re_1)}.$$

According to (36), I_R should be about 0·5. To compute I_R, we need to compare two flows with different Re. This is done carefully by choosing Re_1 and Re_2 close enough (10% difference) so that the flows do not differ qualitatively. We use the averaged slip for calculating f_R and I_R, because it reflects the global character of the flow. Table I clearly confirms the predicted value

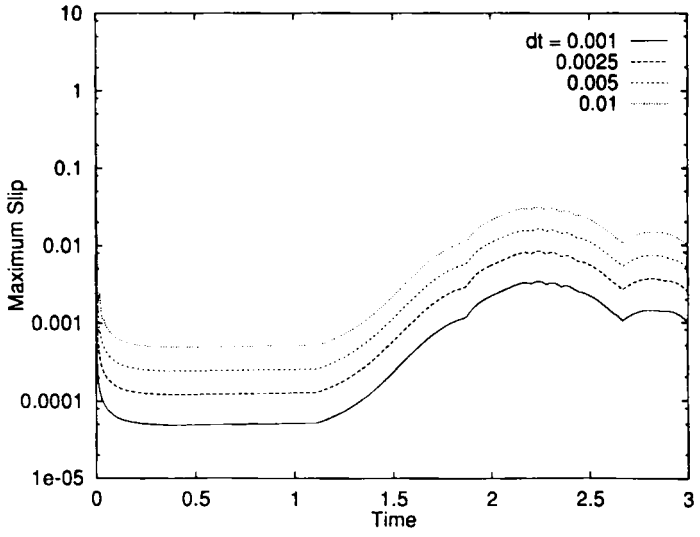

Figure 12. Effect of Δt on maximum slip (see Figure 11 for parameters of grid)

of 0·5 expecially as Re becomes higher. It also presents the L_2-norm relative error in ω_B of the decoupled scheme compared with the fully coupled one using iteration. The index of this error, I_E, is defined similarly to I_R and also has a similar trend. Another indication of the strength of (ω, p) coupling is the number of iterations required to achieve convergence in u_s. As expected, more iterations were needed for lower Re in our tests. A test with $Re = 9500$ shows that (36) is valid for smoothly separated flow, which corresponds to the 'flat' part of the averaged slip in Figure 10. As the slip rises and the flow becomes more complicated, the estimate becomes invalid and the error of decoupling is larger. In Table II we give the errors in boundary vorticity at different times. More importantly, we found that both f_R and hence the error in ω_B due to decoupling seem to be *independent* of grid size when the flow is well resolved. This would imply that the numerical results will not converge to the exact solutions as the grid refines. Therefore the present fractional step decoupled scheme is not suitable for pursuing very-high-resolution computations. On the other hand, for fixed precision simulations in practice the method could be very useful as long as the decoupling error is lower than the discretization error. For example, the largest decoupling error in Table II would be well acceptable if the required precision were 1%. Amazingly, even at $Re = 10$, about the lowest Reynolds number of most practical interest,

Table I. Results obtained with $\Delta t = 0{\cdot}01$ at $t = 1$. f_R is the reduction factor of the averaged slip, I_R is its index; E and I_E are the L_2-norm of relative decoupling error of boundary vorticity and its index respectively

Re	f_R	I_R	E	I_E
10	1·552	0·359	$5{\cdot}093 \times 10^{-3}$	−0·398
100	4·226	0·475	$1{\cdot}992 \times 10^{-4}$	−0·423
1000	12·94	0·497	$7{\cdot}104 \times 10^{-4}$	−0·459
10000	37·49	0·508	$2{\cdot}659 \times 10^{-4}$	−0·466

Table II. L_2-norm of relative decoupling error in boundary vorticity. See legend of Figure 9 for parameters of computation

Time	0·5	1·0	1·5	2·0	2·5	3·0
Error	$6{\cdot}200 \times 10^{-5}$	$6{\cdot}171 \times 10^{-5}$	$1{\cdot}773 \times 10^{-4}$	$1{\cdot}607 \times 10^{-3}$	$1{\cdot}985 \times 10^{-3}$	$1{\cdot}577 \times 10^{-3}$

the decoupling error might be considered as still sufficiently small. It is not feasible to give criterion for whether a decoupled scheme can be used in general, but one can always find this out by comparing the decoupled result with the fully coupled one using the efficient iteration scheme described above.

Therefore we summarize that the present decoupled scheme with dynamic condition is capable of capturing the fine vortex structures of high-*Re* flow, while it can also be used for flow with *Re* as low as 10. The accuracy of short-time simulation depends solely on the grid size, especially in the near-wall and separation regions.

In the present computation the boundary vorticity flux σ is directly affected by the accuracy of computing the slip, and hence so is the pressure solution, since it is computed by integrating the flux. Therefore, again, higher-order methods of computing the slip are desirable.

Our results also clearly indicate the importance of choosing r_∞. For $r_\infty = 5$, although reducing Δr_B leads to better ω_B (Figure 11), it does not improve p_B significantly and might be even worse for separating flow. However, with the same Δr_B, using $r_\infty = 20$ leads to a much better result. It is interesting to note that the difference in σ due to different r_∞ is much less significant than that in p_B, especially when Δr_B keeps the same. Figure 13 shows the C_D variation. For the

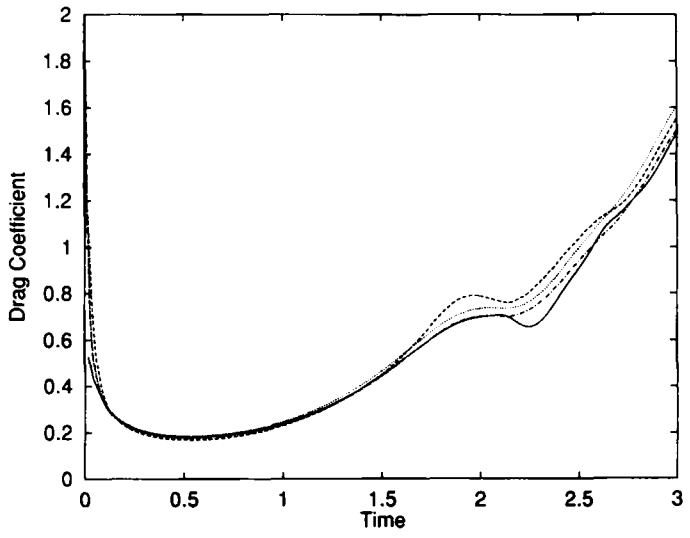

Figure 13. Time variation of drag coefficient with different Δr_B and r_∞ compared with fourth-order result: ———, fourth-order solution; – – –, $\Delta r_B = 0{\cdot}0037$, $r_\infty = 5$; ·····, $\Delta r_B = 0{\cdot}002$, $r_\infty = 5$; – · – · –, $\Delta r_B = 0{\cdot}002$, $r_\infty = 20$

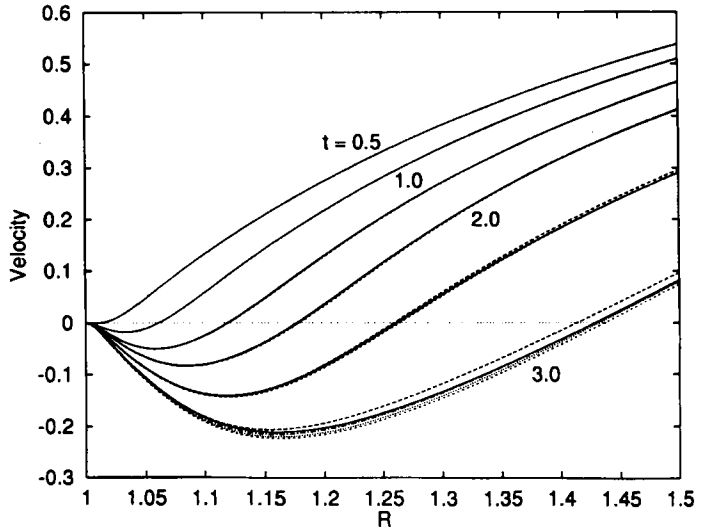

Figure 14. Wake velocity profile obtained with different grid sizes compared with fourth-order results: ———, fourth-order solution; – – –, $\Delta r_B = 0{\cdot}0037$, $\Delta\theta = 0{\cdot}0245$, $r_\gamma = 5$; – – –, $\Delta r_B = 0{\cdot}0037$, $\Delta\theta = 0{\cdot}0123$, $r_\gamma = 5$; ·····, $\Delta r_B = 0{\cdot}002$, $\Delta\theta = 0{\cdot}0123$, $r_\gamma = 5$; – · – · –, $\Delta r_B = 0{\cdot}002$, $\Delta\theta = 0{\cdot}0123$, $r_\gamma = 20$

attached flow where friction drag is dominant, smaller Δr_B makes the result more accurate owing to improving ω_B. When complicated flow separation occurs and a large vortex structure forms behind the cylinder, pressure drag is dominant and r_∞ becomes an important factor in determining the accuracy of C_D. Note that the result in Figure 13 was not expected to converge, because the number of grid points was kept the same although the Δr_Bs are different. This explains the apparent difference between our result and that of AR.

In Figure 14 we compare the wake velocity on the symmetry plane behind the cylinder with the fourth-order solution. The Δr_B effect is not as significant as in other figures. Note that the relatively large error of the result computed with $\Delta\theta = 0{\cdot}0245$ shows that the flow is too under-resolved. The r_∞ effect is clearly seen again at $t = 3$. From this figure and the above observation we conclude that if only the simplest treatment of the far-field condition like ours is to be used, choosing r_∞ far enough is important even for the early-stage computation of a high-Reynolds-number flow.

Finally, we remark that some apparently different treatments of the vorticity boundary condition may in fact be the same. For example, in the method proposed by Hou and Wetton,[25] second-order central difference is used to discretize the spatial derivatives. They also used a local kinematic boundary condition for vorticity, which is derived from the discretized no-slip condition. This leads to nothing but (44′). Since our method of computing the velocity and slip is the same as theirs, when the no-slip condition is satisfied (by using iteration) in our scheme, the local kinematic boundary condition is recovered. Thus the two treatments of the boundary condition become essentially the same (for the present problem). An implication of this observation is that the error analysis of Hou and Wetton may be partially adopted for the present scheme. Also note that the dynamic boundary condition along with the iteration method can be used conveniently in non-fractional step schemes.[30]

5. CONCLUDING REMARKS

The dynamic boundary condition of the Neumann type for vorticity, derived from the Navier–Stokes equation, is the natural choice for the vorticity equation from both mathematical and physical points of view. Owing to the existence of a local equation for the condition, it is easier to analyse and compute with much less uncertainty. Compared with local approximations of kinematic boundary conditions, the pressure can be easily included.

The integral formulation developed for studying the solution structure of vorticity and pressure provides a foundation for deterministic vortex methods and is a perfect way of handling vortex sheet singularities that may exist in the initial condition for vorticity on a solid boundary.

The essential difficulty in applying the dynamic condition is the intrinsic (ω, p) coupling on the boundary. The fact that when the Reynolds number is high (it can be as low as 10), the coupling is weak (about the order of $Re^{-1/2}$) in fractional step methods, is very useful for designing numerical schemes. In fact, we demonstrated that a fully decoupled scheme might give satisfactory results. Whenever necessary, an efficient iteration may be used to recover the global coupling. This method is generally applicable to various vorticity-based schemes and will be most efficient when combined with fast integral methods in computing velocity. The extension of the dynamic condition to three-dimensional problems is straightforward.[30]

The finite difference schemes tested in the present paper suffer from the low-order accuracy of computing the slip. This motivates the construction of higher-order methods. Also, further works, such as testing the performance of the dynamic condition in problems with moving boundaries, are desired.

ACKNOWLEDGEMENTS

This work is supported in part by NASA Langley Research Center under Grant NAG-1-844 and by the Institute of Aeronautics and Astronautics of National Cheng Kung University, Taiwan, China under Cooperative Research Agreement R02-4340-07. We are very grateful for many helpful discussions with Drs. Philip M. Gresho, Christopher R. Anderson, Anthony Leonard, Thomas Y. Hou, Leslie F. Greengard, Claude Greengard, Zhi Y. Lu, Marc B. Reider and Petros D. Koumoutsakos during the progress of the work. In particular, we thank Drs. Anderson and Reider for informing us of their unpublished data on which we relied heavily in testing our numerical schemes, and Dr. Leonard for allowing us to have copies of his students' theses on relevant subjects and their unpublished paper (KLP). We also appreciate the suggestion of one of the referees to test the vorticity–pressure coupling at low Reynolds numbers. The third author (H.-Y. Ma) would like to acknowledge the financial support of J.-M. Wu's Research Fund and the hospitality of the University of Tennessee Space Institute during his visit to the United States in 1992.

REFERENCES

1. P. M. Gresho, 'Imcompressible fluid dynamics: some fundamental formulation issues', *Ann. Rev. Fluid. Mech.*, **23**, 413–53 (1991).
2. P. M. Gresho, 'Some interesting issues in incompressible fluid dynamics, both in the continuum and in numerical simulation', *Adv. Appl. Mech.*, **28**, 45–139 (1992).
3. X. H. Wu, J. Z. Wu and J. M. Wu, 'Efficient Solution of Cauchy–Riemann Equations and its Application to Incompressible Viscous Flow Computations', submitted.
4. C. M. Wang and J. C. Wu, 'Numerical solution of Navier–Stokes problems using integral representation with series expansion', *AIAA J.*, **24**, 1305–1312 (1986).

5. A. J. Chorin, 'Vortex sheet approximation of boundary layers', *J. Comput. Phys.*, **27**, 428–442 (1978).
6. P. Koumoutsakos, A. Leonard and F. Pépin, 'Boundary conditions for viscous vortex methods', *J. Comput. Phys.*, in press.
7. C. R. Anderson, 'Vorticity boundary conditions and boundary vorticity generation for two-dimensional viscous incompressible flows', *J. Comput. Phys.*, **80**, 72–97 (1989).
8. C. R. Anderson and M. B. Reider, 'A high order explicit method for the computation of flow about a circular cylinder', *J. Comput. Phys.*, in press.
9. J. Z. Wu, C. J. Wu and J. M. Wu, 'Vorticity–dilatation boundary conditions for viscous compressible flows', *Proc. 3rd Int. Congr. on Fluid Mechanics*, Cairo, January 1990.
10. J. Z. Wu and J. M. Wu, 'Interaction between a solid surface and a viscous compressible flow field', *J. Fluid Mech.*, **254**, 183–211 (1993).
11. P. M. Gresho and R. L. Sani, 'On pressure boundary conditions for the incompressible Navier–Stokes equations', *Int. j. numer. methods fluids*, **7**, 1111–1145 (1987).
12. J. Z. Wu, 'Generation and absorption of vorticity at arbitrary three-dimensional body surfaces and its dissipation', *Acta Aerodyn. Sinica*, **4**, 168 (1986).
13. J. Z. Wu, J. M. Wu and C. J. Wu, 'A viscous compressible theory on the interaction between moving bodies and flow fields in the (ω, θ) framework', *Fluid Dyn. Res.*, **3**, 203–208 (1988).
14. M. J. Lighthill, in L. Rosenhead (ed.), *Laminar Boundary Layers*, Oxford University Press, Oxford, 1963.
15. J. Z. Wu, X. H. Wu and J. M. Wu, 'Streaming vorticity flux from oscillating walls with finite amplitude', *Phys. Fluids A*, **5**, 1933–1938 (1993).
16. R. Panton, 'The transient for Stockes's oscillating plate: a solution in terms of tabulated functions', *J. Fluid Mech.*, **31**, 819–825 (1968).
17. P. Degond and S. Mas-Gallic, 'The weighted particle method for convection–diffusion equations, Part I: The case of an isotropic viscosity; Part II: The anisotropic case', *Math Comput.*, **53**, 485–526 (1989).
18. F. Pépin, 'Simulation of flow past an impulsively started cylinder using a discrete vortex method', *Ph.D. Thesis*, Caltech, 1990.
19. G. H. Cottet, 'A particle–grid superposition method for the Navier–Stokes equations', *J. Comput. Phys.*, **89**, 301–318 (1990).
20. Z. Y. Lu and T. J. Ross, 'Diffusing-vortex numerical scheme for solving incompressible Navier–Stokes equations', *J. Comput. Phys.*, **95**, 400–435 (1991).
21. J. T. Beale and C. Greengard, 'Convergence of Euler–Stokes splitting of the Navier–Stokes equations', *Res. Rep. RC 18072*, IBM, 1992.
22. P. M. Gresho, 'On the theory of semi-implicit projection methods for viscous incompressible flow and its implementation via a finite element method that also introduces a nearly consistent mass matrix', *Int. j. numer. methods fluids*, **11**, 587–620 (1990).
23. J. Marsden, 'A formula for the solution of the Navier–Stokes equations, based on a method of Chorin', *Bull. Am. Math. Soc.*, **80**, 154–158 (1974).
24. S. C. Hung and R. B. Kinney, 'Unsteady viscous flow over a grooved wall: a comparison of two numerical methods', *Int. j. numer. methods fluids*, **8**, 1403–1437 (1988).
25. T. Y. Hou and B. T. R. Wetton, 'Convergence of a finite difference scheme for the Navier–Stokes equations using vorticity boundary conditions', *SIAM J. Numer. Anal.*, **29**, 615–639 (1992).
26. Z. Y. Lu, 'The diffusion–convection vortex method for solving two-dimensional incompressible Navier–Stokes equation', *Ph.D. thesis*, Cornell University, 1987.
27. J. T. Beale and A. Majda, 'High order accurate vortex methods with explicit velocity kernels', *J. Comput. Phys.*, **58**, 188–208 (1985).
28. X. H. Wu, 'Neumann versus Dirichlet boundary condition for vorticity equation', in B. Antar *et al.* (eds), *Developments in Theoretical and Applied Mechanics*, Vol. 16, The University of Tennessee Space Institute, Tullahoma, TN, 1992, p. IV.SI.32.
29. L. Greengard and J. Strain, 'A fast algorithm for the evaluation of heat potentials', *Commun. Pure Appl. Math.*, **XLIII**, 949–963 (1990).
30. X. H. Wu, 'On vorticity-based methods for incompressible viscous flows', *Ph.D. Thesis*, University of Tennessee, Knoxville, TN, 1994.
31. R. Bouard and M. Coutaneau, 'The early stage of development of the wake behind an impulsively started cylinder for $40 < Re < 10^4$', *J. Fluid Mech.*, **101**, 583–607 (1980).
32. B. P. Leonard, 'A stable and accurate convective modelling procedure based on quadratic upstream interpolation', *Comput. Methods Appl. Mech. Eng.*, **19**, 59–98 (1979).
33. C. W. Shu and S. Osher, 'Efficient implementation of essentially non-oscillatory shock-capturing scheme, II', *J. Comput. Phys.*, **83**, 32–78 (1989).
34. Ta Phuoc Loc and R. Bouard, 'Numerical solution of the early stage of the unsteady viscous flow around a circular cylinder: a comparison with experimental visualization and measurements', *J. Fluid Mech.*, 160, 93–117 (1985).